AGU PUBLICATIONS

JGR

Journal of Geophysical Research: Earth Surface

RESEARCH ARTICLE

10.1002/2014JF003106

Key Points:
- Cross-shore equilibrium shoreline models show skill at shorter-term simulations
- Model-free parameters are predictable and are used to derive parameterizations
- Model skill of a parameterized form of the model remained high

Correspondence to:
K. D. Splinter,
k.splinter@unsw.edu.au

Citation:
Splinter, K. D., I. L. Turner, M. A. Davidson, P. Barnard, B. Castelle, and J. Oltman-Shay (2014), A generalized equilibrium model for predicting daily to interannual shoreline response, *J. Geophys. Res. Earth Surf.*, *119*, 1936–1958, doi:10.1002/2014JF003106.

Received 29 JAN 2014
Accepted 22 AUG 2014
Accepted article online 27 AUG 2014
Published online 22 SEP 2014

A generalized equilibrium model for predicting daily to interannual shoreline response

Kristen D. Splinter[1], Ian L. Turner[1], Mark A. Davidson[2], Patrick Barnard[3], Bruno Castelle[4], and Joan Oltman-Shay[5]

[1]Water Research Laboratory, School of Civil and Environmental Engineering, UNSW Australia, Sydney, New South Wales, Australia, [2]School of Marine Science and Engineering, Plymouth University, Plymouth, UK, [3]United States Geological Survey, Pacific Coastal and Marine Science Center, Santa Cruz, California, USA, [4]Université de Bordeaux, CNRS, UMR 5805 EPOC, Pessac, France, [5]NorthWest Research Associates, Redmond, Washington, USA

Abstract Coastal zone management requires the ability to predict coastline response to storms and longer-term seasonal to interannual variability in regional wave climate. Shoreline models typically rely on extensive historical observations to derive site-specific calibration. To circumvent the challenge that suitable data sets are rarely available, this contribution utilizes twelve 5+ year shoreline data sets from around the world to develop a generalized model for shoreline response. The shared dependency of model coefficients on local wave and sediment characteristics is investigated, enabling the model to be recast in terms of these more readily measurable quantities. Study sites range from microtidal to macrotidal coastlines, spanning moderate- to high-energy beaches. The equilibrium model adopted here includes time varying terms describing both the magnitude and direction of shoreline response as a result of onshore/offshore sediment transport between the surf zone and the beach face. The model contains two coefficients linked to wave-driven processes: (1) the response factor (ϕ) that describes the "memory" of a beach to antecedent conditions and (2) the rate parameter (c) that describes the efficiency with which sand is transported between the beach face and surf zone. Across all study sites these coefficients are shown to depend in a predictable manner on the dimensionless fall velocity (Ω), that in turn is a simple function of local wave conditions and sediment grain size. When tested on an unseen data set, the new equilibrium model with generalized forms of ϕ and c exhibited high skill (Brier Skills Score, BSS = 0.85).

1. Introduction

The world's coastlines mark the interface between the oceans and the continents. Along sandy, wave-dominated stretches of coast, this interface, denoted here as the shoreline, can be quite dynamic; moving landward (eroding) during periods of higher wave energy and moving seaward (accreting) during periods of lower wave energy. The ability to predict both the direction and magnitude of shoreline response to changing wave conditions and therefore the temporal variability in shoreline position is of primary interest to coastal scientists and managers. In particular, predictive models are sought that can provide reliable estimates of the cumulative shoreline response to both short-term storms and longer-term changes in local wave climate.

One of the biggest challenges to achieving this is that the suite of predictive models presently available typically require site-specific calibration. In an effort to expand the general applicability of shoreline models at a wide range of sites where historical data is presently limited, we utilize 12 existing shoreline data sets (herein referred to as "study sites") along six different stretches of coastline to examine the dependence of model coefficients on environmental variables, such as local wave conditions and sediment grain size. This more generalized approach allows for new physical relationships to be derived from more readily available environmental parameters. The broad range of study sites, which include medium to high energy, microtidal to mesotidal environments encompass the majority of commonly observed wave-dominated sandy coastlines where shoreline modeling is most commonly applied.

The choice of model used to predict shoreline change will depend on the governing processes at the site and the timescales over which predictions are required. Both cross-shore and longshore sediment transport determine shoreline response to changing wave conditions. On open coastlines, longshore processes are commonly observed to act over much longer timescales (decades) and most often do not dominate the

seasonal to annual shoreline variability [e.g., *Aubrey*, 1979; *Clarke and Eliot*, 1988; *Hansen and Barnard*, 2010; *Ruggiero et al.*, 2010]. Estimating decadal-scale (and beyond) shoreline change due to gradients in longshore transport is most commonly achieved using 1- (or *n*-) line models [e.g., *Pelnard-Considere*, 1956; *Hanson and Kraus*, 1989; *Ruggiero et al.*, 2010]. In these *n*-line models, the cross-shore profile is assumed to maintain a constant shape and the alongshore gradients in longshore transport result in a cross-shore translation of the profile. *Ruggiero et al.* [2010] found their 1-line shoreline model was skillful at decadal-scale timescales, but had poor skill at the annual scale, which they hypothesized to be dominated by cross-shore processes.

At the other end of the temporal spectrum (i.e., individual storms), cross-shore processes tend to dominate the erosion response and several process-based models such as SBeach [*Larson and Kraus*, 1989] and XBeach [*Roelvink et al.*, 2009] have been used to estimate storm response with an emphasis on quantifying erosion of the upper beach and dune [e.g., *Carley et al.*, 1999; *McCall et al.*, 2010; *Splinter and Palmsten*, 2012; *Splinter et al.*, 2014]. However, bathymetry (or profile) data are rarely available, and if they are, they are typical that they predate the onset of a specific storm by several weeks to months (or even years), which can lead to large uncertainty in the modeled shoreline response [*Splinter and Palmsten*, 2012] and often necessitates "best guess" tuning of model coefficients and limited capacity to apply at other coastal sites.

Encompassing the time frame between individual storms and decadal-scale trends (i.e., seasonal to multiyear) a number of data-driven [e.g., *Frazer et al.*, 2009; *Anderson et al.*, 2010; *Karunarathna and Reeve*, 2013], as well as equilibrium-based semiempirical shoreline models [e.g., *Miller and Dean*, 2004a; *Davidson and Turner*, 2009; *Yates et al.*, 2009, 2011; *Davidson et al.*, 2010, 2013] have been used to model shoreline variability over timescales between individual storms and decadal-scale trends (i.e., seasonal to multiyear). These models require information on shoreline position sampled on the order of monthly and spanning at least 2 years to provide robust calibration of model coefficients [*Splinter et al.*, 2013b]. Most recently, *Pender and Karunarathna* [2013] proposed a method to extend the application of storm scale process models to longer (interannual) timescales. They employed a statistical process-based approach where they utilized a statistical framework [*Callaghan et al.*, 2008] to model waves and were required to separately calibrate XBeach [*Roelvink et al.*, 2009] for the erosion and accretion phases in order to reproduce both phases of the shoreline response signal on interannual timescales.

The focus of this contribution is the application of equilibrium shoreline models to shoreline change driven by cross-shore processes over weekly to seasonal and multiyear timescales. A particular attraction of equilibrium models in this context is the relative transparency in the governing processes compared to data-driven models and that they are also less sensitive than process-based models to uncertainty and/or errors in boundary conditions. Importantly, a growing number of authors [*Miller and Dean*, 2004a; *Davidson and Turner*, 2009; *Yates et al.*, 2009, 2011; *Davidson et al.*, 2010, 2013] have shown that equilibrium-based shoreline models perform well at exposed, open coastlines where significant seasonal (i.e., summer-winter cycle) shoreline variability occurs.

However, not all models of this type have shown a similar degree of skill across a broad range of sites. Both *Miller and Dean* [2004a] and *Yates et al.* [2009] reported on some sites where their equilibrium-based models performed quite poorly. For example, the coarse sand beach at San Onofre, California showed minimal seasonal shoreline change despite the prevailing wave climate being similar to other beaches examined. This difference was hypothesized by *Yates et al.* [2009] to be due to the coarser sediment on San Onofre having the effect of stabilizing the shoreline variability relative to other finer sand sites. While the model of *Yates et al.* [2009] does not explicitly include sediment grain size in its formulation, when the authors applied model coefficients derived from a significantly higher-energy beach but with similar coarse grain size (Ocean Beach, California), the model qualitatively reproduced the subdued seasonal fluctuations observed at San Onofre. It was concluded by *Yates et al.* [2011] that their model coefficients appeared to (implicitly) depend in part on sediment grain size, and this insight now informs the present contribution.

The equilibrium shoreline model proposed by *Davidson et al.* [2013] differentiates equilibrium response of varying beach types through the dimensionless fall velocity (Ω):

$$\Omega = \frac{H_{s,b}}{wT_p}, \tag{1}$$

where $H_{s,b}$ is the significant breaking wave height, w is the settling velocity and is a function of the site-specific median grain size (d_{50}), and T_p is the spectral peak wave period. They applied the new model

Table 1. Summary of Site Statistics[a]

Site	Type	d_{50} (mm)	$\overline{\Omega}$	$\overline{\sigma}_{\Omega_{360}}$	$\overline{\sigma}_{\Omega_{30}}$	$\overline{\sigma}_{\Omega_{360}}/\overline{\sigma}_{\Omega_{30}}$	Primary Wave Buoy ID (Depth, m)
North Head, WA	Exposed	0.2	12.38	4.48	3.69	1.21	NDBC 46029 (145)
Truc Vert, FR	Exposed	0.3[a]	6.19	2.70	2.22	1.22	WWIII(70) and Buoy (54 m)
Gold Coast, QLD	Exposed	0.25	6.17	2.08	1.84	1.13	Gold Coast (17)
Ocean Beach, OB8, CA	Exposed	0.3	5.29	1.78	1.50	1.19	CDIP 029 (550) and SWAN (10)
Ocean Beach, OB5, CA	Exposed	0.3	5.21	1.73	1.48	1.17	
Torrey Pines, CA	Exposed	0.23	5.04	1.89	1.65	1.12	CDIP 100 (554)
Duck, NC	Exposed	0.3[a]	5.06	2.61	2.35	1.11	FRF (17)
Narrabeen, PF1, NSW	Embayed	0.4	4.08	1.36	1.27	1.07	
Narrabeen, PF2, NSW	Embayed	0.4	3.73	1.25	1.17	1.08	
Narrabeen, PF4, NSW	Embayed	0.4	3.75	1.32	1.23	1.07	Sydney (74) and SWAN (15)
Narrabeen, PF6, NSW	Embayed	0.4	3.67	1.31	1.23	1.07	
Narrabeen, PF8, NSW	Embayed	0.4	3.08	1.23	1.15	1.07	
Narrabeen, 2600, NSW	Embayed	0.4	3.67	1.31	1.23	1.07	

[a]Sediment grain size varies considerably at these sites. Previously reported values/means are used here.

to two contrasting beaches on the east coast of Australia: a 20 km long, exposed open beach with a dominant annual shoreline variability (Gold Coast, Queensland) and a 3.5 km long, semiembayed beach where the shoreline is observed to rapidly respond to individual storms throughout the year (Narrabeen-Collaroy, New South Wales). While the model was able to successfully reproduce the contrasting shoreline responses at both these sites, site-specific calibration was still required.

The reality is that the necessary data needed for robust model calibration of any sediment transport model aimed at predicting seasonal to multiyear shoreline change is rarely available. *Long and Plant* [2012] recently proposed a new method for determining site-specific model coefficients. Utilizing an Extended Kalman Filter approach and a sensible starting estimate of model coefficient values, they were able to achieve model coefficient convergence on their synthetic test case using 2 years of monthly sampled data. However, this method has yet to be successfully applied to field data, with one major limitation potentially being a priori knowledge of a reasonable first estimate of each model coefficient. This contribution develops and presents a potential alternative solution. Starting from an existing equilibrium-based model for shoreline change described in further detail in section 3, the calibration process is recast and model coefficients parameterized in terms of commonly available wave and sediment characteristics.

First, we describe the study sites and compare the differing observations of interannual shoreline behavior (section 2). This is followed by a brief description of the existing equilibrium shoreline model that provides the starting point for the analyses that follow (section 3). Shoreline predictions based on site-specific calibration using available historical shoreline data sets for each site are presented and compared in section 4. Intersite variability among model coefficients is then investigated leading to the derivation of generalized forms of model coefficients. Equilibrium shoreline response and the application of the new generalized model at an additional thirteenth site where minimal calibration data were available (i.e., a blind test) are presented in section 5. Finally, a summary of key study findings is provided in section 6, along with encouragement for other researchers to now test the broader application of the generalized model at their specific beaches of interest (Matlab GUI provided on request).

2. Multisite Observations

The 12 study sites used here to explore equilibrium beach response and intersite parameter variability were divided into two distinct categories: (1) exposed open coastlines and (2) semiembayed coastlines (Table 1). Sites were mainly limited to microtidal and mesotidal locations. Fundamentally, the selection and limitation to the use of these specific sites were based on the practical availability to the authors of shoreline time series of a minimum of 5 years duration, sampled at a minimum monthly interval and colocated to suitable wave data. Three sites utilized video-derived (e.g., Argus: [*Holman et al.*, 2003]) shorelines, while the remaining nine were collected using standard survey techniques, such as Real-Time Kinematic-GPS. Where possible, shoreline data were alongshore averaged (Table 2) to limit the influence of local short-scale

Table 2. Summary of Survey Data and Wave Sources[a]

Site	Date Range	Number of Surveys	Alongshore Average (m)	Type	Estimated Uncertainty In Measurement (m)	Frequency	Shoreline Contour wrt MSL (*zRel*, m)	Mean Spring Tidal Range (ΔTide, m)
North Head, WA	2006–2012	176	1000	Argus	2	Biweekly	MHW (0.81)	2.3
Truc Vert, FR	2005–2013	121	350-1200	Survey	2	Monthly	MHW (1.5)	3.7
Gold Coast, QLD	2001–2008	329	1000	Argus	5	Weekly	MSL (0.2[a])	1.5
Ocean Beach, CA	2004–2013	110–114	500	Survey	2	Monthly	MHW (0.64)	1.83
Torrey Pines, CA	2003–2009	80	-	Profile[b]	5	Monthly	MSL (0)	1.62
Duck, NC	2000–2006	58	230	Profile	2	Monthly	MHW (0.65)	1.2
Narrabeen, NSW	2005–2012	94	-	Profile	5	Monthly	MHW (0.7)	2
Narrabeen, NSW	2005–2012	434	400	Argus	2	Weekly	MHW (0.7)	2

[a]Gold Coast is derived from the Argus Timex image closest to MSL. Using an average wave height of 1.2 m, setup is roughly 0.2 m.
[b]Data from Torrey Pines was digitized from Figures 4 and 9 of *Yates et al.* [2009] at roughly monthly intervals. Where the shoreline was interpolated from a surface, estimated uncertainty was taken as 2 m, whereas if the shoreline was extracted from a single image or from a profile, the uncertainty was taken as 5 m.

alongshore variability (e.g., beach and/or mega cusps). The study site locations are shown in Figure 1 and composed of two stretches of coastline in Australia, three in the United States, and one in France. Characteristics of each site are summarized in Tables 1 and 2 and discussed in more detail below.

Three summary environmental statistics for each site are reported in Table 1. The first is the temporal mean (over the record of available data) of the dimensionless fall velocity (Ω, equation (1)). The temporal mean ($\overline{\Omega}$) can be used to infer the dominant (modal) beach state after *Wright and Short* [1984]. The remaining two are based on the standard deviation of Ω at yearly (defined by a calendar year and denoted as $\sigma_{\Omega_{360}}$) and monthly (defined by a calendar month and denoted as $\sigma_{\Omega_{30}}$) intervals. The temporal mean of these statistics over the entire record length ($\overline{\sigma}_{\Omega_{360}}$, $\overline{\sigma}_{\Omega_{30}}$) is then determined for each site. The mean yearly standard deviation ($\overline{\sigma}_{\Omega_{360}}$) characterizes the variability in the forcing wave climate over a year, while the mean monthly standard deviation ($\overline{\sigma}_{\Omega_{30}}$) characterizes the variability at the timescales of individual storms. It is expected that $\overline{\sigma}_{\Omega_{360}}/\overline{\sigma}_{\Omega_{30}} \geq 1$. A large ratio of $\overline{\sigma}_{\Omega_{360}}/\overline{\sigma}_{\Omega_{30}}$ indicates a site that is dominated by seasonal fluctuations in wave steepness. As the ratio of $\overline{\sigma}_{\Omega_{360}}/\overline{\sigma}_{\Omega_{30}}$ approaches unity, we expect a site that experiences both

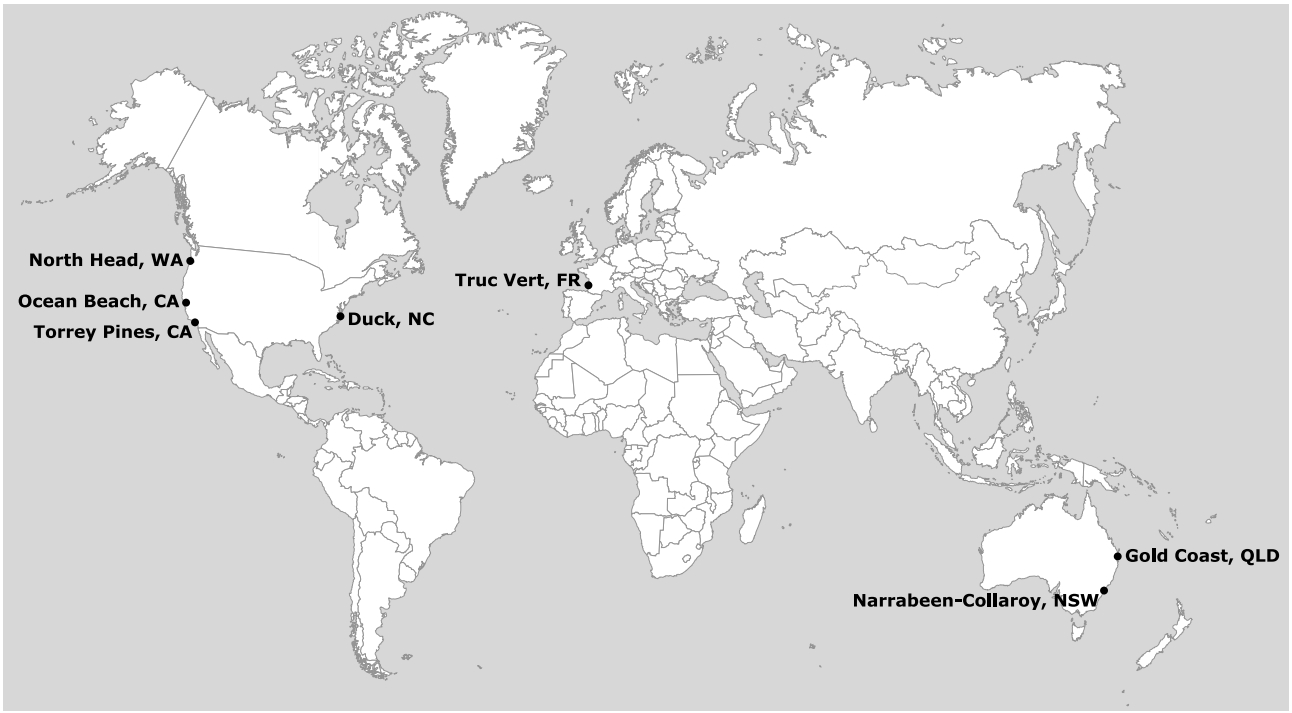

Figure 1. Map of the seven geographic locations encompassing the 13 transects/sites used in the present paper.

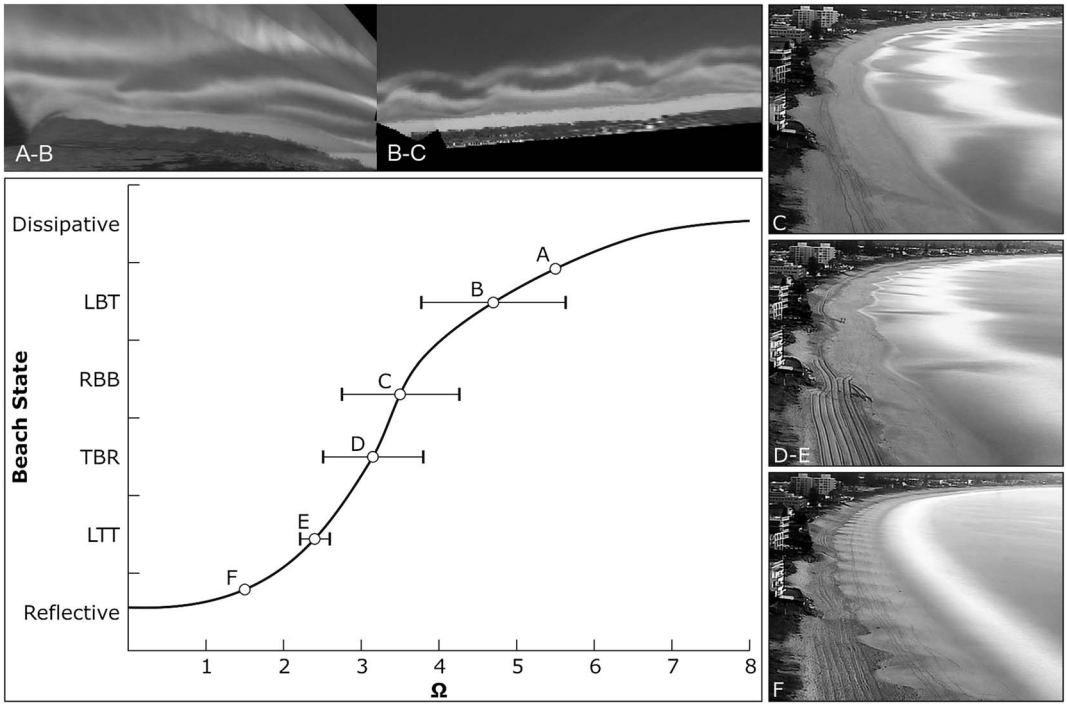

Figure 2. Example beach states with respect to dimensionless fall velocity as described in *Wright and Short* [1984]. (A-B) Dissipative at North Head, Washington; (B-C) longshore bar-trough (LBT) and rhythmic bar-beach (RBB) at Gold Coast, Queensland; (C) RBB; (D-E) transverse-bar-rip (TBR) and low-tide terrace (LTT); (F) reflective. C-F are from Narrabeen, New South Wales.

high- and low-steepness waves throughout the year (i.e., a storm-dominated site) and a shoreline time series that mirrors this. The ratio can be used to characterize site-specific beach state. Higher-energy beaches with a dominant seasonal cycle ($\overline{\sigma}_{\Omega_{360}}/\overline{\sigma}_{\Omega_{30}} > 1$) are anticipated to remain more stable and in a higher-energy state, while more intermediate and low-energy sites with a large variability in wave conditions at shorter timescales ($\overline{\sigma}_{\Omega_{360}}/\overline{\sigma}_{\Omega_{30}} \sim 1$) will likely respond quickly to storms and more rapidly return to these lower energy states. To encapsulate these differing physical behaviors, a weighted mean dimensionless fall velocity ($\overline{\Omega}_r$) is derived:

$$\overline{\Omega}_r = \overline{\Omega}\frac{\overline{\sigma}_{\Omega_{360}}}{\overline{\sigma}_{\Omega_{30}}}. \quad (2)$$

2.1. Exposed Open Coastlines

2.1.1. Benson Beach (North Head), Washington, USA

Benson Beach is a 3 km long, fine sand ($d_{50} \sim 0.2$ mm) exposed beach (Tables 1 and 2), located between the North Head headland and the north jetty of the Columbia River. The site is mesotidal with a mean spring tide range (ΔTide) of 2.3 m (Table 2). The nearshore is characterized by a multibar system (typically between two and four sandbars) and is the most dissipative site available to this study (Figure 2), with $\overline{\Omega} = 12.38$ (Table 1). During the summer, the inner sandbar moves onshore and attaches to the shoreline, while in the winter, the beach face is cut and sand is transported offshore to the sandbars. Both the shoreline and the wave climate exhibit a highly seasonal and well-correlated signal [*Ruggiero et al.*, 2009]. Longshore transport is estimated at 0.4 M m^3/yr to the north. Winter waves (and storms) are typically from the NW, while the smaller summer waves generally arrive from the SW. The mean yearly standard deviation in dimensionless fall velocity ($\overline{\sigma}_{\Omega_{360}}$) is 4.48, and the mean monthly standard deviation in dimensionless fall velocity ($\overline{\sigma}_{\Omega_{30}}$) is 3.69. This highly seasonal site has a ratio of $\overline{\sigma}_{\Omega_{360}}/\overline{\sigma}_{\Omega_{30}} = 1.21$, which is the second highest of all sites examined, resulting in a weighted mean dimensionless fall velocity ($\overline{\Omega}_r$) = 15.04.

Dredge material was placed within the intertidal system near the jetty in the summers of 2008 (~96,000 m^3) and 2010 (~281,000 m^3). Analysis of the dredge material indicates that the sand was moved offshore forming a new sandbar shortly after placement during the first storm and that the mean high water (MHW)

shorelines during and post placement lie within the natural envelope of shoreline variability at this site. To limit the impact on the analysis presented below of these localized nourishments, as well as the presence of the jetty, this study utilized the 1 km alongshore averaged mean high water (MHW) shoreline centered approximately 2 km north of the jetty (Table 2). Wave data (86%) was obtained from wave buoy NDBC 46029 (Columbia River Bar) located in 145 m of water and gap filled with NDBC 46041 (Cape Elizabeth) located in 114 m of water. These buoys were chosen as they are considered deep water for periods (T_p) less than 12 s (65% of the data), and they cover the entire monitoring period of the North Head site. The correlation between the two buoys for wave height was $R = 0.95$. Further information about this site can be obtained at www.planetargus.com/north_head.

2.1.2. Truc Vert, France

Truc Vert is a medium-grained ($d_{50} \sim 0.3$ mm [*van Rooijen et al.*, 2012]), sandy beach located in the southwest of France. The site is mesotidal to macrotidal, with a mean spring tide range (ΔTide) of 3.7 m and a moderate wave climate ($\overline{\Omega} = 6.19$, Tables 1 and 2). There exists a strong seasonal dependence in waves ($\overline{\sigma}_{\Omega_{360}} = 2.70$) and the resulting position of the MHW shoreline. The ratio of $\overline{\sigma}_{\Omega_{360}}/\overline{\sigma}_{\Omega_{30}}$ is 1.22, and is the highest for all sites included in this study. The weighted $\overline{\Omega}_r$ is 7.55. The beach morphology (Figure 2) is typically double barred, with the inner, intertidal sandbar classified as transverse bar and rip [*Senechal et al.*, 2009] and the outer bar as crescentic [*Castelle et al.*, 2007a]. Around Truc Vert Beach, the longhsore drift is about 0.3 M m^3/yr with a negligible alongshore variability along this stretch of coastline suggesting a limited influence of the longshore transport on the overall shoreline evolution [*Idier et al.*, 2013].

MHW shorelines were derived from topographic survey data, which were sampled every 2–4 weeks (Table 2), with a 1 year gap in 2008 [*Castelle et al.*, 2014]. The MHW contour was alongshore averaged over the extent of the available survey data to minimize the local influence of mega cusps. Between 2003 and 2008, the alongshore extent of the surveys was 350 m, and was extended to 750 m in 2008 and then again to 1200 m in 2012 [*Castelle et al.*, 2014]. Wave data at this site were based on modeled WaveWatchIII output every 3 h from grid point 1°30′W, 44°30′N, which is located 34 km SW of the study site in 70 m water depth. *Davidson et al.* [2011] tested a similar form of the shoreline model used here and found that temporally degrading the wave data (i.e., increasing the time step) by up to 2 days did not cause a significant decrease in model skill at the sites tested. As such, using the 3-hourly WaveWatchIII output in the absence of hourly measured buoy data at this site is acceptable. The 11.5 years of WWIII data is corrected via linear regression fit with approximately 5 years of interspersed buoy data located in 54 m of water as detailed in *Castelle et al.* [2014].

2.1.3. Narrowneck (Gold Coast), Queensland, Australia

The Gold Coast is located along the east coast of Australia near the Queensland-New South Wales state border. The Gold Coast site is a microtidal (ΔTide = 1.5 m), medium sand size ($d_{50} \sim 0.25$ mm), 20 km long, straight beach, exposed to waves from a range of directions (Tables 1 and 2). The site is located approximately 2 km updrift (south) of an artificial surfing reef and outside the influence of this nearshore structure. Predominant wave direction is from the S-E and results in an estimated average net northerly longshore transport at Narrowneck of 0.5 M m^3/yr [*Delft*, 1970; *Patterson*, 2007]; however, this can vary significantly from year to year [*Patterson*, 2007; *Splinter et al.*, 2012]. On average, summer waves are smaller and more easterly, while winter waves are larger and have a larger southerly component. The wave climate of the SE coast of Australia is influenced by El-Niño Southern Oscillation (ENSO) timescale phenomena, as well as extreme storms, such as East Coast Lows and tropical cyclones [*Allen and Callaghan*, 1999]. The nearshore morphology at this site is typically a double-barred system [*van Enckevort et al.*, 2004] and ranges from alongshore uniform sandbars during high wave events to crescentic bars and rip-dominated low-tide terraces under prolonged mild wave conditions (Figure 2). Shoreline variability along the Gold Coast displays an annual cyclic pattern related to changes in seasonal mean wave height ($\overline{\sigma}_{\Omega_{360}} = 2.08$) [*Davidson and Turner*, 2009; *Splinter et al.*, 2011b]; however, since 2005, there has been an observed shift in shoreline variability from a predominant seasonal pattern to more storm driven with episodic erosion (Figure 4). While $\overline{\Omega} = 6.17$ at the Gold Coast is comparable to that at Truc Vert, this site has a larger storm-dominated standard deviation, and the second lowest ratio of $\overline{\sigma}_{\Omega_{360}}/\overline{\sigma}_{\Omega_{30}} = 1.13$ among the exposed sites examined, resulting in $\overline{\Omega}_r = 6.95$. Weekly mean sea level (MSL) shorelines (Table 2) were derived from video images and averaged over a 1 km length of coastline to limit the influence of local rip-horn variability. Wave data for this study was obtained from the Gold Coast buoy located in 18 m of water directly offshore from this study site.

2.1.4. Ocean Beach, California, USA

Ocean Beach is a 7 km, west facing, medium-grained (d_{50} ~ 0.3 mm), microtidal (ΔTide = 1.83 m), sandy beach located directly south of the entrance to San Francisco Bay (Tables 1 and 2). The site is swell dominated and exposed to strong alongshore tidal currents due to tidal movement in and out of the Bay [*Barnard et al.*, 2012]. Tidal currents are generally larger at the north end of Ocean Beach (transects north of OB10), while waves generally have a larger impact on the southern section of the beach [*Barnard et al.*, 2012], which contains an erosion hotspot (i.e., an area of increased erosion compared to the surrounding beach) between transects OB3 and OB4 [*Barnard et al.*, 2012]. The majority (~ 45%) of the waves are from the northwest (300°–330°N); however, 50% of winter waves (November–March) are from the west (270°–300°N) and in the summer, long-period swell can occasionally also come from the S-SW (180°–210°N) [*Eshleman et al.*, 2007] with an $\overline{\Omega}$ ~ 5.25. Ocean Beach is strongly controlled by gradients in longshore transport [*Hansen et al.*, 2013b]; however, those gradient patterns only seem to change on multidecadal timescales, primarily as a result of the large-scale changes of the ebb-tidal delta morphology [*Hansen et al.*, 2013a]. Longshore transport has been roughly estimated in the area to be between 0.1 and 0.3 M m^3/yr; however, over the timescale considered here, cross-shore processes dominate the seasonal to subdecadal shoreline response.

To minimize the potential influence of a known erosion hot spot [*Hansen and Barnard*, 2010] at the southern end of Ocean Beach and the strong tidal currents at the north end of this site, the analysis presented here focuses on the central 2 km of the beach around transects OB5 and OB8 as presented in *Yates et al.* [2011]. The MHW contour was extracted from available survey data and alongshore averaged over a 500 m section for each of the transects to remove the influence of localized alongshore variability and to conform with similar work at this site by *Yates et al.* [2011] (Table 2). Available wave data is sourced from the deep water CDIP 029 buoy located approximately 80 km west of Ocean Beach. Local waves are influenced by the Fallon Islands (40 km west) and a substantial ebb tidal delta (~150 km^2) at the mouth of the Bay, which have been observed to cause substantial alongshore gradients in wave energy [*Eshleman et al.*, 2007; *Hansen et al.*, 2013b]. To account for these features, an existing look-up table derived from a calibrated SWAN output presented in *Eshleman et al.* [2007] and *Hansen et al.* [2013b] and verified in *Eshleman et al.* [2007] against inshore observations was used here to transform the deep water waves into the −10 m contour directly offshore of OB5 and OB8. The shoreline and inshore wave data vary on a seasonal timescale ($\overline{\sigma}_{\Omega_{360}}$ ~ 1.75). Ocean Beach has a larger ratio of $\overline{\sigma}_{\Omega_{360}}/\overline{\sigma}_{\Omega_{30}}$ ~ 1.18 and is midrange among all the exposed sites examined, resulting in a weighted mean dimensionless fall velocity of $\overline{\Omega}_r$ ~ 6.2.

2.1.5. USACE Field Research Facility, Duck, NC, USA

The beach at Duck is an east facing, intermediate ($\overline{\Omega}$ = 5.06), microtidal (ΔTide = 1.2 m), medium-grained (d_{50} ~ 0.2–0.3 mm) open exposed coastline located on the Outer Banks of North Carolina. The area experiences a net southerly littoral drift; however, the wave climate typically has a seasonal signal, with smaller waves during the summer months typically arriving from the southeast and larger, winter waves arriving from the northeast. The area can be impacted by hurricanes in late summer-early fall and large winter storms (Nor'easters) that can cause significant storm surge and erosion. The annual standard deviation in the dimensionless fall velocity ($\overline{\sigma}_{\Omega_{360}}$ = 2.61) is similar to that observed at the Truc Vert site but also has one of the largest storm-scale variability standard deviations ($\overline{\sigma}_{\Omega_{30}}$ = 2.35). As a result, the ratio of $\overline{\sigma}_{\Omega_{360}}/\overline{\sigma}_{\Omega_{30}}$ = 1.11 at the Duck site is the lowest of all exposed open coastlines available to this study, resulting in $\overline{\Omega}_r$ = 5.61 (Table 1). The nearshore morphology (Figure 2) is typically double-barred, dynamic and ranges from low-tide terraces to alongshore uniform sandbars [*Lippmann and Holman*, 1990].

The beach at Duck is the most complex site utilized in this study due to both natural and anthropogenic influences on the shoreline. In addition to the influence of hurricanes and large Nor'easter storms, located at this site is a 560 m long research pier that significantly influences the nearshore morphology and sediment transport immediately adjacent [e.g., *Miller and Dean*, 2004a]. Both longshore and cross-shore processes influence the shoreline. *Plant et al.* [1999] and *Miller and Dean* [2003] observed an increasing alongshore uniform component of variability with distance offshore and that the shoreline was dominated by variability at timescales greater than 1 year. The shoreline is considered to be stable over the long term [*Birkemeier et al.*, 1985] with a mean annual range in cross-shore shoreline position less than 3 m [*Alexander and Holman*, 2004].

The profile data used in this study were collected at the US Army Corps of Engineers Field Research Facility (USACE FRF). The survey area extends approximately 600 m on either side of the FRF pier; however, to

minimize the more localized influences of the pier on shoreline data, only the MHW shorelines that were at least 350 m south of the pier were used and alongshore averaged over 250 m (Table 2). Previous analysis by *Miller and Dean* [2004a] of the Duck profile data from 1981 to 2002 indicated that roughly 70% of the observed shoreline variability over this 250 m section was alongshore uniform. Wave data was obtained from the FRF 17 m buoy (55%) and gap filled with NDBC 44014 (Virginia Beach) located in 95 m of water. Waves from the FRF 17 m buoy were reverse shoaled to deep water prior to gap filling for consistency. The correlation of wave height between the two data sets was $R = 0.59$.

2.2. Semiembayed Coastlines

2.2.1. Narrabeen and Collaroy, NSW, Australia

Narrabeen and Collaroy beaches are located on the Northern Beaches region of Sydney. The beaches are microtidal (ΔTide = 2 m), coarse sand ($d_{50} \sim 0.4$ mm), east facing, swash aligned, and occur within a single 3.5 km embayment (Tables 1 and 2). The two adjacent beaches are bounded by prominent rocky headlands: Warriewood Headland to the north and Long Reef Headland to the south. The beaches are storm dominated, with the northern (Narrabeen) end exposed to, and the southern (Collaroy) end sheltered from, the predominant south to south-easterly wave climate. An alongshore gradient in wave energy within the embayment exists resulting in $\overline{\Omega}$ ranging from 3.08 at the southern end of Collaroy beach to 4.08 at the northern end of Narrabeen beach. Typically, the smaller, summer waves have a more easterly component than the larger, more southerly winter waves, similar in this respect to Narrowneck (section 2.1.3). The ratio of $\overline{\sigma}_{\Omega_{360}}/\overline{\sigma}_{\Omega_{30}} = 1.07$ is the lowest among all the study sites included here and highlights the larger storm (short term) contribution of wave variability along Narrabeen-Collaroy (Table 1). The weighted mean dimensionless fall velocity around the embayment is within the most dynamic intermediate range ($3.28 \leq \overline{\Omega}_r \leq 4.37$). Hourly wave data were obtained from the Sydney buoy located in 74 m water depth, 11 km SE of the site. To account for wave refraction into the embayment and the resulting alongshore gradient in wave height, these offshore observations were then used as input into a look-up table of calibrated SWAN-modeled output at the −15 m contour around the embayment.

The beach morphology within the Narrabeen-Collaroy embayment is dynamic, ranging from dissipative, with a longshore uniform sandbar during major storms, through all four intermediate beach states (Figure 2) during milder wave conditions. Five profile locations along the embayment have been consistently surveyed on a monthly basis using standard survey techniques since 1974 at historical profiles PF1, PF2, PF4, PF6, and PF8; however, the necessary directional wave data are only available since 1992. To be consistent with the time span of all data sets available to this study (2000s), profile data over a 7 year period coinciding with the availability of Argus camera-derived shorelines (NB2600) were used here (Table 2). The profile data utilize the MHW contour, are not alongshore averaged, and sampled monthly. In contrast, the Argus MHW shoreline is sampled weekly and alongshore averaged over 400 m to limit the influence of small-scale alongshore variability. Comparing sites PF6 and NB2600 (Figure 5), which overlap the same alongshore location, the reader can see short-lived accretionary events (e.g., mid-2010) that are present in the profile data (PF6) but have been averaged out by the alongshore smoothing in NB2600. As a benchmark, the average alongshore standard deviation of the shoreline at NB2600 was 1.5 m, which if applied at each profile within the embayment, would add an additional 3 m of uncertainty onto the shoreline position.

It has been previously observed that both cross-shore and alongshore transport processes influence shoreline position within the Narrabeen-Collaroy embayment at annual and longer (i.e., ENSO) timescales [*Short and Trembanis*, 2004; *Ranasinghe et al.*, 2004]. *Harley et al.* [2011] has shown that at Narrabeen-Collaroy, 60% of the observed shoreline variance is due to cross-shore processes (the first EOF) linked to the temporal variation of wave height and 26% of the shoreline variance is linked to longshore processes (beach rotation in the second EOF). PF1 is the most exposed site and is located at the north end of Narrabeen. PF4 is located near the center of the embayment and the pivot point of observed embayment rotation [*Harley et al.*, 2011] and as such, cross-shore processes have been previously assumed to be the driving factor in shoreline change. PF8 is the most sheltered and southern location at Collaroy considered.

3. An Equilibrium-Based Shoreline Model: *ShoreFor*

3.1. Formulation

The *ShoreFor* model was first presented in *Davidson et al.* [2013] and is used here as the basis to explore the more general applicability of equilibrium shoreline modeling and intersite comparison of model coefficients. *ShoreFor* is based upon the principal that cross-shore-dominated shorelines migrate toward a

time-varying equilibrium position [e.g., *Miller and Dean*, 2004a; *Davidson and Turner*, 2009; *Yates et al.*, 2009; *Davidson et al.*, 2010]. By this approach, the rate of shoreline change (dx/dt; m/s) is simply defined as follows:

$$\frac{dx}{dt} = c(F^+ + rF^-) + b. \tag{3}$$

The rate of shoreline change model (equation (3)) includes two wave-driven coefficients (c, ϕ) and a linear trend term (b). The first wave-driven parameter is the rate parameter (c; $m^{1.5}\ s^{-1}\ W^{-0.5}$). The second wave-driven parameter is the response factor (ϕ; days) that is optimized during the calculation of the equilibrium dimensionless fall velocity (Ω_{eq}, equation (8)) described below. The linear term (b; m/s) is included here to acknowledge longer-term processes not explicitly included in the present form of the model (e.g., gradients in longshore transport, cross-shelf sand supply, etc.), which may be captured by a constant rate over long time frames. Where these processes cannot be captured by the linear term (or the wave-driven component), the model does not resolve the shoreline response.

The key forcing term in (3) is subdivided into accretionary (F^+) and erosional (F^-) components multiplied by a ratio (r, no units) to encapsulate that accretionary and erosion responses are governed by different processes [*Miller and Dean*, 2004a; *Yates et al.*, 2009; *Splinter et al.*, 2011a]. For clarity, r will be referred to as the erosion ratio as it is attached to the erosion forcing term (F^-). The erosion ratio is not a free model coefficient, but determined within the model based on the balance between accretion and erosion forcing (F, $(W/m)^{0.5}$) such that no trend in the integrated forcing results in no trend in the shoreline evolution due to cross-shore transport processes. The erosion ratio in (3) is numerically evaluated in the model as:

$$r = \left| \frac{\sum_{i=0}^{N} \langle F_i^+ \rangle}{\sum_{i=0}^{N} \langle F_i^- \rangle} \right|, \tag{4}$$

where $\|$ indicates the absolute value, $\langle\rangle$ indicates a numerical operation that removes the linear trend but preserves the record mean, and N is the total record length.

The rate of shoreline response (dx/dt) is dependent on the magnitude of forcing (i.e., wave energy flux, P) available to move sediment and the direction of shoreline response is based on the disequilibrium (the deviation between the present and equilibrium position). The forcing term (F) is defined as

$$F = P^{0.5} \frac{\Delta\Omega}{\sigma_{\Delta\Omega}}, \tag{5}$$

where P (Watts) is the breaking wave energy flux:

$$P = EC_g. \tag{6}$$

$E = 1/16\rho g H_{s,b}^2$ (Newton/m) is the significant wave energy at breaking (assuming a breaking parameter, $\gamma = 0.78$) and $C_g = \sqrt{gh_b}$ is the shallow water group velocity (m/s), where h_b (m) is the depth at breaking defined as $h_b = H_{s,b}/\gamma$. As described in *Davidson et al.* [2013], *Davidson et al.* [2010] showed that results were not sensitive to the exponent on P (i.e., 0.5) in equation (5); therefore, it was sensibly chosen to agree with previous work, such as *Yates et al.* [2009] whereby the shoreline rate of change is linearly related to the wave height (H).

The dimensionless fall velocity disequilibrium term ($\Delta\Omega$) in (5) is given by

$$\Delta\Omega = \Omega_{eq} - \Omega, \tag{7}$$

and is a function of the time-varying equilibrium condition (Ω_{eq}, equation (8)) and the instantaneous dimensionless fall velocity (Ω, equation (1)). Note that the standard deviation of $\Delta\Omega$ (denoted $\sigma_{\Delta\Omega}$) is used to normalize $\Delta\Omega$ in (5), such that the rate parameter (c) and wave energy flux (P) determine the magnitude of the shoreline response (dx/dt), rather than $\Delta\Omega$. The sign of $\Delta\Omega$ determines the direction of shoreline change (erosion or accretion) and is used to partition F^+ and F^- in (3) and (4).

While *ShoreFor* is an equilibrium shoreline model, the time-varying equilibrium position (Ω_{eq}, equation (8)) is based on beach state (rather than a shoreline position). Therefore, changes in Ω_{eq} directly link surf zone

onshore-offshore sediment transport to the resulting shoreline response. Following the approach outlined in *Davidson et al.* [2013], the time-varying equilibrium beach state was based on the formulation proposed by *Wright et al.* [1985]:

$$\Omega_{\mathrm{eq}} = \left[\sum_{i=1}^{2\phi} 10^{-i/\phi}\right]^{-1} \sum_{i=1}^{2\phi} \Omega_i 10^{-i/\phi}, \tag{8}$$

where i is the number of days prior to the present time and the response factor (ϕ) is a model coefficient. The response factor represents the number of days in the past when the weighting factor decreases to 10%, 1%, and 0.1% at ϕ, 2ϕ, and 3ϕ days prior to present day. The present formulation incorporates all past beach state information for the past 2ϕ days (i.e., with a minimum weighting factor of 1%). Therefore, the equilibrium condition (Ω_{eq}) is constantly evolving and maintains a weighted "memory" of antecedent surf zone and shoreline conditions.

Additionally, a representative response factor (ϕ_r, days), is included here for comparison with other studies where a running mean is more commonly used. The representative response factor is determined by transforming the weighted filter used in (8) to the equivalent filter length if a running mean were used:

$$\phi_r = \left[\sum_{i=1}^{2\phi} 10^{-i/\phi}\right]^{-1} \sum_{i=1}^{2\phi} [0 : \mathrm{d}t : 2\phi] 10^{-i/\phi}. \tag{9}$$

For the purpose of intersite comparison of model coefficients, wave energy flux (P, equation (6)) and dimensionless fall velocity (Ω, equation (1)) were calculated using the depth-limited significant breaking wave height ($H_{s,b}$) since this is judged to best represent the local wave forcing that is assumed to drive cross-shore shoreline change at each site. At the two sites (Ocean Beach, CA, USA and Narrabeen, NSW, Australia) where significant refraction and alongshore variation in wave height was expected, SWAN modeling was used to refract waves inshore. To standardize the method used to determine wave-breaking statistics at all sites, waves were first reverse-shoaled to deep water from their respective depths (Table 1) and then breaking wave height ($H_{s,b}$; m), applying shoaling only, was calculated following *Komar* [1974]:

$$H_{s,b} = 0.39 g^{1/5} (T_p H_{o,s})^{2/5}, \tag{10}$$

where g (m/s^2) is the acceleration due to gravity, and $H_{o,s}$ (m) is the deep water significant wave height. On swell-dominated coasts with large seasonal variations in T_p as is observed along the California coastline, utilizing the breakpoint, rather than the deep water conditions, can shift the temporal variability of the magnitude in breaking wave heights at a beach and must be considered.

3.2. Model Expectations and Limitations

The model formulation presented above describes the temporal variation in shoreline position due to changing wave conditions, and as such, is best suited for locations where waves are the primary driver of shoreline response. The model does not account for short-scale processes such as alongshore variable bar welding, beach cusp formation, or rip embayments/horns. As such, sites where shoreline data can be alongshore averaged to limit the impact of these short-scale processes are preferred. Sheltered coastlines, or those that experience large tidal variation are also influenced by the changes in mean water level not included in the present form of the model. The exclusion of water level also precludes the impacts of changes in mean water level due to climatological impacts, such as storm surge, El Nino–Southern Oscillation (ENSO), and sea level rise. Where these processes potentially have a constant linear impact on shoreline change (e.g., sea level rise), these can be modeled by the linear trend term (b). Shoreline change due to gradients in longshore transport and/or onshore/offshore feeding/loss of sand may also be captured in the present formulation by the linear trend term; however, there is no discrimination of the impact of these processes on shoreline change from each other. When these processes are not constant in time (such has multidecadal embayment rotation), this variability is not accurately modeled. As such, it is anticipated that this modeling approach is best suited on open microtidal to mesotidal coastlines, exposed to waves over time frames of years to decades.

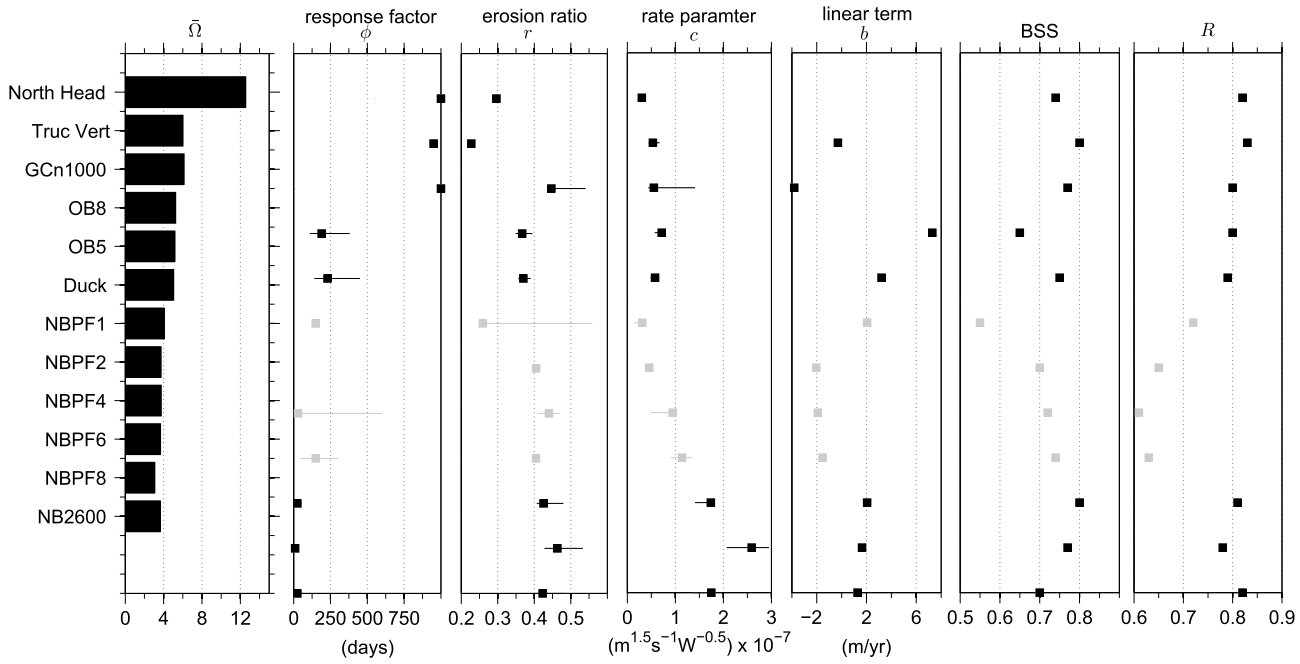

Figure 3. Summary statistics from all model runs. Grey indicates that model skill is not considered significant enough to be included in further analysis. Significance is defined here as having an $R \geq 0.70$ and a BSS ≥ 0.6. Horizontal lines indicate the range of coefficient values where R^2 did not decrease by more than 10% of maximum. (left to right) Mean dimensionless fall velocity ($\bar{\Omega}$); response factor (ϕ); erosion ratio (r); rate parameter (c); linear term (b); model Brier Skills Score (BSS); and model Correlation (R).

4. Model Results

In this section we present the site-specific calibration of model coefficients and the overall skill of the generic equilibrium shoreline model at each of the 12 study sites followed by the derivation of model coefficients using easily obtainable site information such as waves and sediment grain size. Figure 3 provides a summary of these results. As the focus of this work is intersite comparison of model coefficients, the full available data set at each site was used for model calibration. For a more detailed discussion on model skill in relation to calibration length and validation on unseen data, the reader is referred to *Davidson et al.* [2013] and *Splinter et al.* [2013b].

Three summary statistics are presented in Table 4 and are all based on a nominal 30 day sampling interval to facilitate unbiased intersite comparison. The first parameter used for intercomparison is correlation (R) between observed shoreline time series and model predictions. The second method uses the Brier Skills Score [*Sutherland and Soulsby*, 2003] and takes into account measurement error in the data (Δx):

$$\mathrm{BSS} = 1 - \frac{\sum \left[|x - x_m| - \Delta x\right]^2}{\sum (x - x_b)^2}, \tag{11}$$

where x is the observed shoreline, x_m is the modeled shoreline, and x_b is the baseline model. Here we use x_b equal to the linear trend of the data in order to determine when model skill is truly due to the model capturing the shoreline response due to varying cross-shore wave processes, rather than the simple linear trend (i.e., the time integration of b in (3)). Positive BSS indicates that the model is an improvement over the baseline linear trend, and descriptive skill values exceeding 0 are summarized in Table 3.

Table 3. Summary of Qualitative Skill Assessments Based On Brier Skill Scores (BSS) and Normalized Mean Square Error (NMSE)

Skill	BSS	NMSE
Poor	0–0.3	> 0.8
Fair	0.3–0.6	0.6–0.8
Good	0.6–0.8	0.3–0.6
Excellent	> 0.8	< 0.3

The third metric reported in Table 4 is the normalized mean square error (NMSE) that compares the error variance to the observed variance. NMSE is chosen over root-mean-square error (RMSE) as the individual data-model results are normalized

Table 4. Skill Assessment of All Model Results Based On Individual Calibration to Full Data Set[a]

Site	R	BSS	NMSE	Significant
North Head, WA	0.82	0.85	0.33	Y
Truc Vert, FR	0.83	0.83	0.31	Y
Gold Coast, QLD	0.80	0.80	0.36	Y
Ocean Beach, OB8, CA	0.80	0.80	0.40	Y
Ocean Beach, OB5, CA	0.79	0.81	0.37	Y
Duck, NC	0.72	0.68	0.48	N
Narrabeen, PF1, NSW	0.65	0.72	0.58	N
Narrabeen, PF2, NSW	0.61	0.72	0.63	N
Narrabeen, PF4, NSW	0.63	0.76	0.60	N
Narrabeen, PF6, NSW	0.81	0.76	0.35	Y
Narrabeen, PF8, NSW	0.78	0.70	0.39	Y
Narrabeen, 2600, NSW	0.82	0.78	0.33	Y

[a]Significant skill is defined as having an $R \geq 0.70$ and BSS ≥ 0.6.

by the variance of the observations (x) at each site, thereby providing a superior method for intersite comparison. Here the formula utilized by *Miller and Dean* [2004b] and *Splinter et al.* [2013b] is adopted:

$$\mathrm{NMSE} = \frac{\sum(x - x_m)^2}{\sum x^2}. \qquad (12)$$

A value of NMSE = 0 indicates that the model perfectly captures all data points, while an NMSE = 1 indicates the error variance (numerator in equation (12)) is equal to the variance of the observations (denominator in equation (12)) and therefore the model has no skill. Similar to the BSS, a range of descriptive NMSE skill is summarized in Table 3.

4.1. Exposed Open Coastlines

With the exception of the Duck data set, the observed shorelines from the remaining five exposed sites exhibit a strong seasonal signal with larger waves driving shoreline erosion and beach recovery (shoreline accretion) during prolonged periods of lower-steepness waves (Figure 4). The *ShoreFor* equilibrium model characteristically performed well at these five exposed beach sites, with correlation (R) typically exceeding 0.8 (Figure 3), and skill classified as "excellent" (Table 3) based on BSS and "good" based on NMSE (Table 4). Encouragingly, the equilibrium shoreline model, *ShoreFor*, captured the strong seasonal signal observed at five of the sites, as well as the contrasting anomalous years at North Head (i.e., 2009, Figure 4). From 2005 until the end of the available monitoring in 2008, the Gold Coast site appears to have transitioned from a seasonally dominated shoreline to one that experiences more episodic erosion (Figure 4). The large erosion event in 2006 is linked to a cluster of storms together with the onset of a new net offshore migration event and outer bar decay [*Castelle et al.*, 2007b; *Ruessink et al.*, 2009]. Further analysis is needed to confirm if a second erosional event combined with a net offshore migration and bar decay occurred in 2008. The equilibrium-based model is still capable of capturing this transition; however, the magnitude of storm response is not always captured and the model marginally lags response post 2005.

Three of the exposed beach sites: Gold Coast ($\overline{\Omega} = 6.14$); Truc Vert ($\overline{\Omega} = 6.02$); and North Head ($\overline{\Omega} = 12.56$) had optimized response factors (ϕ) close to 1000 days (Figure 3), equating to representative response factors (ϕ_r, equation (9)) around 400 days. Recalling that ϕ_r represents the equivalent number of days in the past that is used in a running mean filter of the wave data to determine the equilibrium condition. This indicates that the equilibrium condition (equation (8)) is roughly equal to the annual mean dimensionless fall velocity and that the observed dominant signal of shoreline variability and the rate of cross-shore sediment exchange at these locations is primarily driven by seasonal (or longer) variability in wave steepness oscillating about this mean (Figure 4). The two California sites at Ocean Beach ($\overline{\Omega} = 5.18 - 5.26$), along with the Duck site ($\overline{\Omega} = 5.06$) had optimized ϕ values between 150 and 230 days (ϕ_r between 62 and 95 days), indicating that there is a steep drop off in optimized response factors (ϕ) as beaches transition between a stable dissipative state ($\overline{\Omega} \geq 6$) and the higher-energy intermediate states ($4 \leq \overline{\Omega} \leq 6$). The representative response factors (ϕ_r) found in this study agree with previous results reported by *Hansen and Barnard* [2010] at Ocean Beach, where a 90 day running mean of the offshore significant wave height showed a similar cyclic pattern to the first two temporal modes of shoreline variability.

Across all the exposed sites investigated here, the range of the rate parameter (c; $m^{1.5}\ s^{-1}\ W^{-0.5}$) varied by a factor of 2 between 3.02×10^{-8} at the most dissipative site (North Head, $\overline{\Omega} = 12.56$) and 7.17×10^{-8} (Ocean Beach, $\overline{\Omega} = 5.26$, Figure 3). The erosion ratio (r; equation (4), Figure 3) also varied significantly between 0.23 (Truc Vert) and 0.45 (Gold Coast). Exploration of the dependency of these parameters (ϕ, c, and r) on quantifiable environmental variables is discussed in more detail in section 4.3. The linear trend term (b; equation (3), Figure 3) ranged from eroding at a rate of −4.52 m/yr (North Head) to accreting at a rate of 7.29 m/yr (OB8) and accounts for observed long-term trends in shoreline change not related to changes in wave height and period.

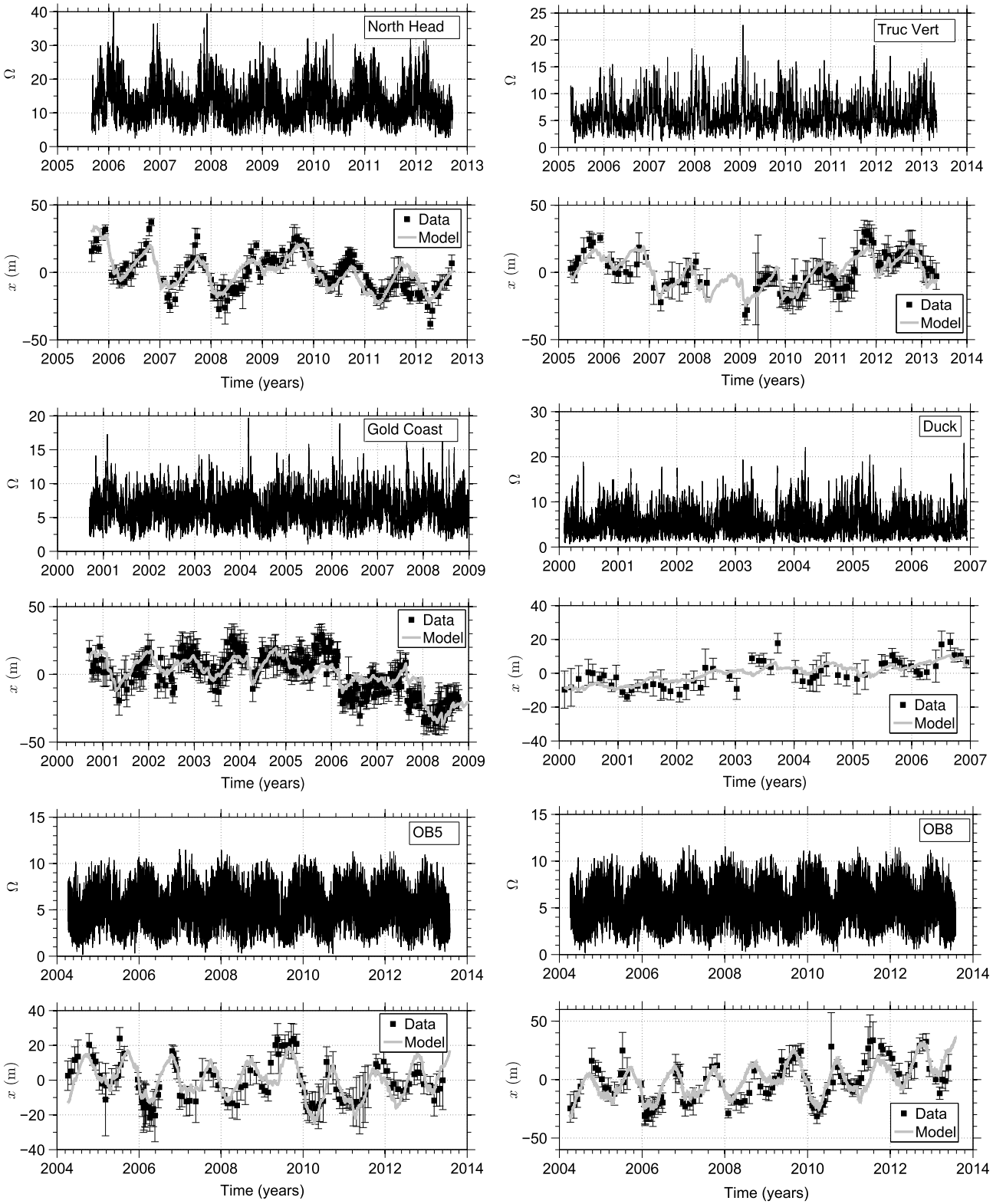

Figure 4. Equilibrium shoreline response for exposed, open-beaches. Subfigures are labelled by individual site and in each the following applies: (top) The time series of dimensionless fall velocity; (bottom) the observed shoreline data with the mean removed (solid black square with error bars representing both the uncertainty in the measurement technique and, where available, the time-varying alongshore standard deviation of the mean shoreline as described in Table 2) and the model prediction (solid grey line).

4.2. Semiembayed Coastlines

The semiembayed sites at Narrabeen and Collaroy beaches consisted of five survey profiles and a sixth Argus-derived shoreline all obtained over the same 7 year period. The profile data are not alongshore averaged and therefore uncertainty associated with localized variability such as beach cusps and localized accretion/erosion are not accounted for.

At Narrabeen-Collaroy, storms occur throughout the year and the beach, which modally is classified as a rip-dominated beach, responds more rapidly to these changes in wave conditions via the rapid exchange of sediment between nearshore sandbars and the beach face [*Davidson et al.*, 2013]. The equilibrium model parameters are summarized in Figure 3. Model skill was good (Table 4) at all six sites (Figure 5). Optimized response factors (ϕ) were 1–2 orders of magnitude lower than at the exposed open coastlines, ranging from 10 days at the most sheltered site (PF8), to the record mean ($\geq$1000 days) at the most exposed site (PF1). The shorter ϕ values indicate the beach has a very short memory of past beach state conditions, while the more energetic northern end of the beach with a longer ϕ value indicates that the beach is oscillating around the annual mean wave condition. This alongshore variation of ϕ as a function of wave exposure (i.e., $\overline{\Omega}$) is expected based on the timescales of sediment exchange between the beach face and the nearshore under reflective, intermediate, and more dissipative conditions [*Wright et al.*, 1985].

Values of the rate parameter (c; Figure 3) ranged from 4.56×10^{-8} at the most exposed semiembayed site (PF1) to 2.59×10^{-7} at the most sheltered site considered here (PF8). While the more exposed site (PF1) had a c value which was midrange to that found at the exposed coastlines, the variability among the semiembayed sites was 3 times larger than the range observed at the exposed sites. However, the erosion ratio (r) was relatively constant around the embayment and ranged between 0.40 and 0.46 (Figure 3). The linear trend term (b), which captures the physical processes not presently encapsulated in the cross-shore equilibrium shoreline model ranged from −2.03 m/yr at the northern exposed end (PF1) to 2.05 m/yr at the southern end (PF6), indicating that the embayment was most likely undergoing a counterclockwise rotation during this 7 year period.

4.3. Intersite Comparison of Model Coefficients

Eight sites (Figures 3–4) in this study were considered to be sufficiently skillful ($R \geq 0.70$, BSS ≥ 0.6, NMSE ≤ 0.4) to examine if the (so far) site-specific wave-driven coefficients vary in a systematic manner across the broad spectrum of coastal settings represented in this study. Second, the goal is to determine if new parameterized forms can be simply derived from readily available environmental characteristics, such as local wave conditions and sediment grain size and therefore potentially reduce the need for extensive site-specific calibration data sets in the future.

4.3.1. Wave-Driven Model Coefficients

The two wave-driven model coefficients (refer to section 3) that are optimized during the calibration process are ϕ and c. The response factor (ϕ) describes the dominant response time of cross-shore sediment exchange at a specific site, while the rate parameter (c) represents the efficiency with which waves induce cross-shore sediment transport resulting in onshore/offshore sandbar migration and shoreline change. Based on the dominant nearshore morphology and sediment characteristics at each site, it is anticipated that different types of beaches will respond differently to similar changes in wave conditions. For example, it is commonly observed that energetic coastlines (higher $\overline{\Omega}$), such as North Head and Truc Vert, exhibit one or multiple offshore sandbars that effectively dissipate incident band wave energy in the surf zone. Shoreline variability at these sites is typically observed to respond at the timescales of the dominant seasonal variation in wave climate (large $\overline{\sigma}_{\Omega_{360}}/\overline{\sigma}_{\Omega_{30}}$), as sediment is cyclically transferred between offshore bars and the beach face. Conversely, more sheltered coastlines (lower $\overline{\Omega}$), such as Narrabeen and Collaroy, tend to have more rhythmic nearshore sandbar features closer to the shoreline. Sediment exchange between the subaerial beach and nearshore is typically more rapid. As a result, shoreline variability tends to predominate at the storm timescale, rather than the seasonal scale.

Figure 6 shows the optimized filter values (ϕ) versus the weighted mean dimensionless fall velocity ($\overline{\Omega}_r$, equation (2)) for all eight sites. It is observed that as $\overline{\Omega}_r$ increases, so does the response factor (ϕ), indicating that the shorelines along dissipative beaches tend to respond to the seasonal changes in wave climate and are more resilient to individual storms, while the shorelines of lower energy, more reflective beaches rapidly respond to changes in wave energy. To synthesize these observations, a best fit curve is shown in Figure 6

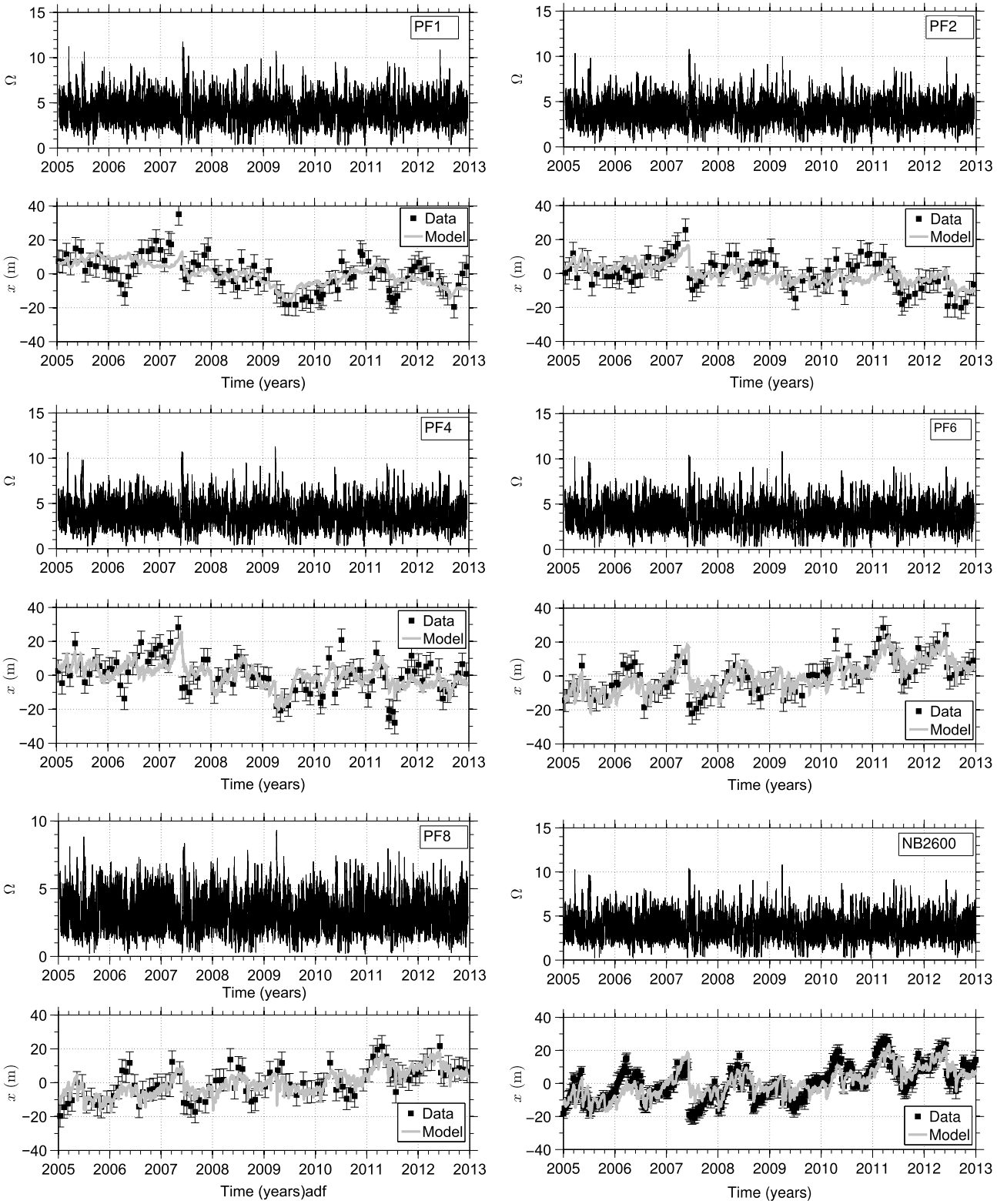

Figure 5. Equilibrium shoreline response for semiembayed coastlines. Subfigures are labelled by individual site and in each the following applies: (top) The time series of dimensionless fall velocity; (bottom) the observed shoreline data with the mean removed (solid black square with error bars representing both the uncertainty in the measurement technique and, where available, the alongshore standard deviation of the mean shoreline as described in Table 2) and the model prediction (solid grey line).

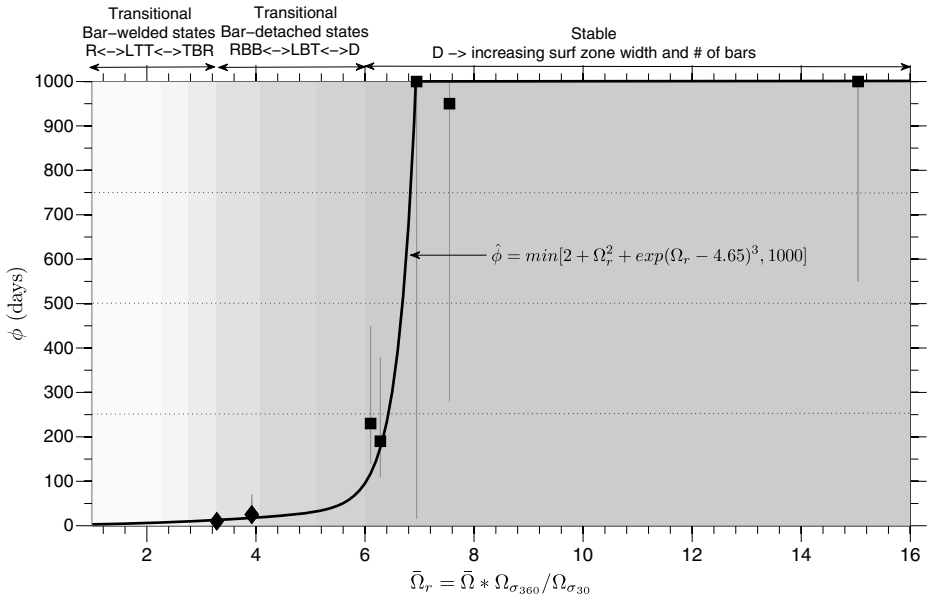

Figure 6. Optimized values of the response factor (ϕ) as a function of weighted dimensionless fall velocity ($\overline{\Omega}_r$). Exposed coastlines are in solid squares, semiembayed beaches are shown as solid diamonds. Grey vertical bars represent the range of ϕ where model skill (R^2) remained within 10% of maximum. $R^2 = 0.99$. A best fit parameterization of the response factor ($\hat{\phi}$, solid line) as described in (13) is also shown. $\hat{\phi}$ was sensibly capped at 1000 days to limit past data requirements, while not impacting the filtered Ω time series (Ω_{eq}).

using the weighted dimensionless fall velocity. The parameterized response factor ($\hat{\phi}$), where ($\hat{}$) indicates a parameterized value is given by

$$\hat{\phi} = min\left[2 + \overline{\Omega}_r^2 + \exp\left(\overline{\Omega}_r - 4.65\right)^3, 1000\right], \tag{13}$$

where "exp" represents the exponential function (e). The parameterization $\hat{\phi}$ fits the data well ($R^2 = 0.99$, Figure 6) and can be usefully subdivided into three main categories of shoreline response. When beaches are modally in the reflective state ($\overline{\Omega}_r \leq 1$), the response factor ($\hat{\phi}$) is near constant. As $\overline{\Omega}_r$ increases through the transitional/intermediate beach states of bar-attached and bar-detached states, $\hat{\phi}$ increases at a rate of $\overline{\Omega}_r^2$ (Figure 6). As the beach transitions into more dissipative states ($\overline{\Omega}_r \geq 4.65$) there is an exponential increase in $\hat{\phi}$. For highly dissipative beaches ($\overline{\Omega}_r \geq 6$), the shoreline is again observed to be more stable and the response factor ($\hat{\phi}$) becomes independent of $\overline{\Omega}_r$ and optimizes at the order of 1000 days (i.e., several years) duration. A cutoff of 1000 days was selected here as a practical upper bound of past data required, as this accounts for the past 2000 (i.e., 2ϕ) days in calculating Ω_{eq} (equation (8)). Further extending this upper bound does not significantly alter Ω_{eq} [*Davidson et al.*, 2013].

The rate parameter (c) ranged from 3.02×10^{-8} at the most dissipative site (North Head) to 2.59×10^{-7} at the most sheltered site (Collaroy, NBPF8), suggesting an inverse relationship between c and mean offshore forcing ($\overline{\Omega}$). Across all study sites, larger values of the rate parameter (c) were also associated with smaller values of the response factor (ϕ) (Figure 3). As the present model formulation has a nonlinear dependency between these two terms, they are likely interdependent; however, the normalization of $\Delta\Omega$ in (5) by $\sigma_{\Delta\Omega}$ limits this influence.

There are several physically based explanations for this observed inverse relationship of c and $\overline{\Omega}$. First is the physical shape of the profile of the beach. As $\overline{\Omega}$ increases, beaches tend to not only be located along coastlines exposed to higher waves but also be composed of finer sand (smaller d_{50}) and exhibit milder nearshore beach slopes. By the breakpoint hypothesis, a sandbar will develop at the cross-shore location of the depth-limited breaking waves [e.g., *Dean*, 1973], and as such, on milder sloping beaches waves break further offshore, resulting in wide surf zones that effectively dissipate wave energy over the one to multiple sandbars that exist. This hypothesized efficiency to dissipate wave energy further offshore results in less energy available to move sand onshore/offshore in the nearshore and cause shoreline change. Conversely,

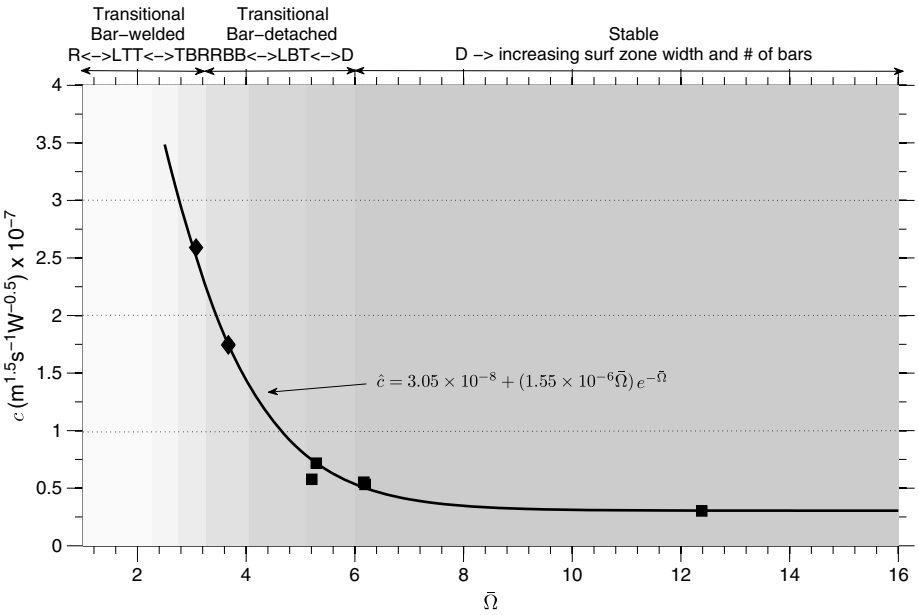

Figure 7. Optimized values of the rate parameter (c) as a function of mean dimensionless fall velocity ($\overline{\Omega}$). Exposed coastlines are in solid squares, semiembayed beaches are shown as solid diamonds. A best fit parameterization of the rate parameter (denoted $\hat{c}$) as described in (14) is also shown. The extension of the parameterization beyond observations for low values of $\overline{\Omega}$ is not included as there is insufficient data. $R^2 = 0.99$.

on steeper, coarse sand beaches, with smaller waves (low $\overline{\Omega}$), the breaker line is closer to shore, inducing sediment transport and the efficient and rapid exchange of sand between inshore sandbars and the beach face. Also, beaches characterized by lower $\overline{\Omega}$ are typically associated with more complex surf zone morphology, while higher values of $\overline{\Omega}$ typically are associated with alongshore linear (multiple) sandbars [*Wright and Short*, 1984]. Complex surf zone morphology can induce circulation that moves sediment onshore more efficiently than a linear system [*Splinter et al.*, 2011a], thus also increasing c for lower $\overline{\Omega}$.

The true explanation is likely to be a combination of the mechanisms mentioned above. Curve fitting to the available data, a parameterized rate parameter ($\hat{c}$) is derived:

$$\hat{c} = 3.05 \times 10^{-8} + (1.55 \times 10^{-6}\overline{\Omega})e^{-\overline{\Omega}}. \quad (14)$$

This empirical relationship for $\hat{c}$ ($R^2 = 0.99$, Figure 7) is consistent with the available observations that for larger values of the mean dimensionless fall velocity associated with dissipative beaches ($\overline{\Omega} > 6$), the rate parameter converges to a constant value ($\hat{c} \rightarrow 3.01 \times 10^{-8}$). In contrast, during the transitional phases as the surf zone sandbars transition from bar-welded states to bar-detached states ($1 \leq \overline{\Omega} \leq 6$, Figure 7) there is an exponential decay in $\hat{c}$ that is hypothesized to relate to the enhanced efficiency in cross-shore transport under complex surf-zone morphology. Albeit that this empirically derived parameterization fits the data quite well, the extension of the present curve beyond observations (particularly for $\overline{\Omega} \leq 2$) should be taken with caution. Reflective beaches are generally less dynamic than intermediate beaches because they are nearly always coincident with lower energy levels (F, equation (5)) and coarser sediments (larger d_{50}), which both inhibit the mobility of the shoreline (equation (3)). As such, as $F \rightarrow 0$, $dx/dt \rightarrow 0$ with no requirement that $\hat{c} \rightarrow 0$ as well. However, allowing the parameterized rate parameter to exponentially increase as $\overline{\Omega} \rightarrow 0$ would suggest that reflective beaches are highly mobile, despite the usual coarse sand present. As such, new observations in this low-energy reflective beach state are needed to confirm and/or refine this anticipated environmental dependency of $\hat{c}$ for $\overline{\Omega} \leq 2$.

Significantly, the adoption of these two wave-driven parameterizations ($\hat{\phi}$: equation (13) and $\hat{c}$: equation (14)) may provide the potential to utilize this equilibrium-based approach in predicting shoreline variability and change at a site based on local environmental variables (waves and sediments), rather than calibration to a preexisting (or, more likely, nonexistent) shoreline monitoring data set. An example of this approach is given in section 5.2.

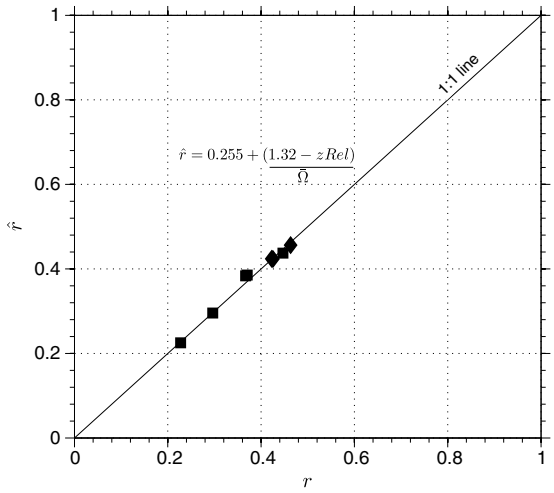

Figure 8. Parameterization of the erosion ratio ($\hat{r}$) as a function of shoreline contour elevation with respect to MSL (*z*Rel) and mean dimensionless fall velocity ($\overline{\Omega}$) as described in (15). $R^2 = 0.99$. Exposed coastlines are in solid squares, semiembayed beaches are shown as solid diamonds.

4.3.2. The Erosion Ratio (*r*)

The erosion ratio defines the balance of the integrated accretion and erosion forcing (equation (4)) which would result in no trend in the shoreline for the optimized response factor (ϕ). While *r* is not a free parameter in the equilibrium model, large intersite dependency was observed ($0.23 \leq r \leq 0.46$) and therefore some further discussion is warranted. Similar to the response factor and the rate parameter, the erosion ratio is likely to be influenced by the efficiency of onshore transport and offshore bar morphology [*Splinter et al.*, 2011a], whereby lower *r* values correspond to a system that is more resistant to erosion. Study sites where the shoreline contour with respect to MSL (*z*Rel, Table 2) was close to zero (Gold Coast), had the highest *r* values ($r = 0.45$, Figure 3), while the larger tidal range (ΔTide, Table 2) sites, which also utilized the MHW shoreline and were also the most dissipative ($\overline{\Omega} \geq 6$) sites available for inclusion in this work (Truc Vert ($r = 0.23$) and North Head ($r = 0.30$) had some of the lowest *r* values. Based on curve fitting to the available data, a relationship to describe the erosion ratio is as follows:

$$\hat{r} = 0.255 + \frac{1.32 - z\text{Rel}}{\overline{\Omega}}. \tag{15}$$

The parameterization for $\hat{r}$ ($R^2 = 0.99$, Figure 8) was the most complex of the three parameterizations. The explicit inclusion of tidal range (ΔTide) in (15) was also explored; however, the additional complexity of $\hat{r}$ for a small increase in model skill was not justified for the data sets available here. However, for completeness the parameterized form for $\hat{r}$ including tidal range is given ($R^2 = 1.00$):

$$\hat{r} = 0.072(1 + \Delta\text{Tide}) + \frac{2.01 - 1.78z\text{Rel}}{\overline{\Omega}}. \tag{16}$$

Similar to the parameterized form of the rate parameter ($\hat{c}$), there was an inverse dependence of the parameterized erosion ratio ($\hat{r}$) on $\overline{\Omega}$. Like $\hat{c}$, it is hypothesized that this is due to the varying efficiency of sand transfer between the beach face and the surf zone sandbars. The shorelines of dissipative beaches (large $\overline{\Omega}$) are resilient to small changes in wave height as sand is predominantly moved during the slow cross-shore migration of offshore sandbars, while on more reflective/terrace beaches (small $\overline{\Omega}$), more rapid exchanges of sediment between the beach face and the inshore sandbars dominate.

Similarly, (15) suggests that the parameterized erosion ratio decreases with increasing shoreline contour elevation (*z*Rel). Shoreline contours around MSL exhibit localized high variability, with potentially large horizontal excursions induced by minimal net sediment transport causing sandbars to weld and detach from the shoreline [e.g., *Castelle et al.*, 2014]. In contrast, elevation contours higher up the beach face are less influenced by these small and rapid exchanges of sediment around MSL. This observation is likely more important on meso-macro tidal sites where significant quantities of sand can be transported within the intertidal zone over a single tide cycle, resulting in a very "noisy" MSL shoreline contour, as such, the MHW contour is preferred over the MSL contour when available [*Castelle et al.*, 2014].

5. Discussion

5.1. Equilibrium Shoreline Response

From the presentation above of data-model comparisons obtained across a broad spectrum of sandy beach settings on three continents, it is evident that the equilibrium-based approach to model shoreline response

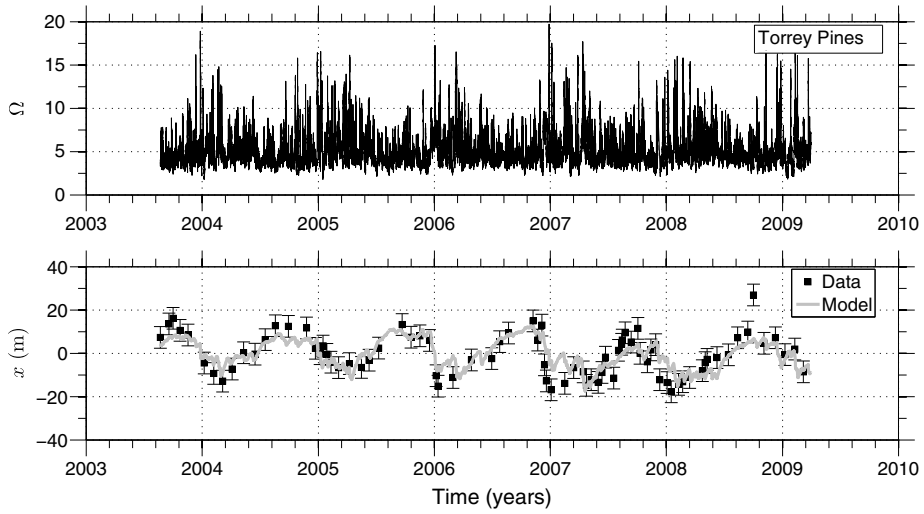

Figure 9. Model results for Torrey Pines utilizing the parameterizations for the response factor ($\hat{\phi}$, equation (13)) and the rate parameter ($\hat{c}$, equation (14)). Model skill was ranked as "good" to "excellent": R = 0.80, BSS = 0.85, and NMSE = 0.37.

was successful at capturing the seasonal to decadal-scale response of shorelines to time-varying wave conditions. As evidenced in Figures 4, 5, and 9, the model did not capture the full magnitude of all the accretion and erosion events. These accretionary "spikes" may be attributed to short-lived bar welding events, but some, including the 2008 event at Torrey Pines, remain unexplained [*Yates et al.*, 2009]. The under-estimation of erosion within the model during some events may be attributed to increased erosion due to large storm surge. A clear example of this is in the model results for Narrabeen mid-2007 (Figure 5). Wave heights during this East Coast Low exceeded 3 m for 65 h, with a maximum recorded water level (tide and surge) of 0.365 m above mean sea level. The impact of high water levels, large setup due to the large waves, and the storm lasting several tidal cycles resulted in significant dune erosion. The observed wave conditions, which are modeled in the disequilibrium term ($\Delta\Omega$) along with the forcing (F) were not enough to cause this magnitude of erosion in the model. While the model under-estimated erosion during this event, the model also did not predict the magnitude of the rapid accretionary response of the shoreline post storm. Had the model predicted this magnitude of shoreline accretion poststorm, the model and data would have potentially continued to diverge post mid-2007. Instead, the observed wave conditions produced a smaller disequilibrium and forcing in the model that resulted in only minor shoreline change over the next 2–3 months. This resulted in a modeled shoreline position of −5 m to −10 m below the record average (Figure 5), NB2600. When the observed shoreline eventually recovered from the storm and returned to being in relative equilibrium with the prevailing wave conditions, the model begins to track the data again by August 2007. This suggests that while the equilibrium model may not capture every event, the formulation is capable of self-correcting in time.

The equilibrium concept was most successful at the exposed open coastline sites ($R \geq 0.79$, BSS ≥ 0.80, NMSE ≤ 0.4; Table 4) where a change in wave steepness is anticipated to be the key driver in daily to seasonal shoreline variability. These open-coast sites are characterized by long response factors (ϕ), on the order of the seasonal to annual cycle (representative response factors, $\phi_r = 62 - 414$ days), with changes in shoreline position and wave steepness well correlated (Table 4).

The exception to this high model skill across all the exposed open coastlines available to this study was the model performance at the Duck, NC site. Previous analysis and application of an equilibrium shoreline model by *Miller and Dean* [2004a] at this same Duck site highlight how two adjacent stretches of coastline on either side of the pier can exhibit very different shoreline behavior. While the multiyear onshore and offshore movement of sandbars has been demonstrated to be well correlated to changes in offshore wave height at the Duck site [e.g., *Plant et al.*, 1999], the results presented here are consistent with *Miller and Dean* [2004a]. As other researchers have reported, the lower model skill may be attributed to several complex processes influencing the shoreline at this Duck site. *Plant and Holman* [1996] previously observed that shoreline variability at the complex Duck site was dominated by rhythmic alongshore shoreline variability

with length scales of order 1 km that progressed at an average rate of 1 m/day. While these features were modulated at a seasonal cycle, the alongshore averaged shoreline (as was used in this study) did not contain a significant annual cycle. *List et al.* [2006] also observed that shoreline change immediately adjacent (±5 km) to the FRF pier was quite small compared to the full Duck-Hatteras, NC cell, and that for this region of North Carolina, shoreline response was not significantly correlated to offshore peak wave height.

The equilibrium approach presented here performed well ($0.61 \leq R \leq 0.82$; Table 4) at the semiembayed beach sites for the period of survey data available here. As can be observed in Figure 5, the six survey sites around the Narrabeen-Collaroy embayment spanning the full range of higher- to lower-energy intermediate beach states indicate that the embayment underwent a slight anticlockwise rotation over the 7 year period of observations. The northern profiles (PF1, PF2) exhibited a net erosive trend, while the southern profiles (PF6, PF8) and alongshore averaged Argus-derived shoreline (NB2600) accreted during this period as indicted by the linear trend term (*b*, Figure 3). Contrary to initial expectations, the more sheltered (southern) end of the study embayment exhibited higher skill than the more exposed (northern) end. Two explanations for this range of skill are proposed. First, that the more sheltered end is less susceptible to longer-term (multiyear) rotational shifts in wave energy. Along the Australian East Coast it has been well documented that semiembayed coastlines, such as Narrabeen-Collaroy, adjust to this change in modal wave direction [*Ranasinghe et al.*, 2004], but the magnitude of change is less pronounced at the more sheltered ends [*Harley et al.*, 2011]. Second, shoreline response at the more sheltered ends of embayments along this stretch of coastline are primarily driven by the change in wave exposure due to the seasonal rotation between summer (more easterly) and winter (more southerly) waves as is observed in the seasonal variation of the shorelines presented in Figure 5. Despite these regional-scale rotational effects, the equilibrium-based approach was still considered skillful (BSS $\geq$ 0.7 and NMSE $\leq$ 0.6; Table 4), supporting the concept that at the timescales of wave-driven cross-shore sediment transport, the equilibrium concept driven by cords-shore processes predominantly controlled the shoreline position at all locations within the embayment. It is anticipated that the inclusion of an additional longshore component to this equilibrium-based approach would likely assist by allowing the (sometimes contrasting) processes of longshore and cross-shore sediment transport to both contribute to the resulting shoreline response [*Harley et al.*, 2011; *van de Lageweg et al.*, 2013].

5.2. A Generalized Form of the Model

A robust model that can be reliably used and widely applied to predict shoreline variability and change with minimal need for site-specific calibration is a sought after tool by coastal scientists and engineers alike. Here we test the performance of the equilibrium-based *ShoreFor* model (equation (3)) utilizing the new empirically derived parameterizations for the wave-driven components presented above: the response factor ($\hat{\phi}$, equation (13)) and the rate parameter ($\hat{c}$, equation (14)). While the parameterization for the erosion ratio ($\hat{r}$, equation (15)) could also be included in (3), it is not a free parameter and is instead determined within the model to maintain the balance between onshore and offshore transport under equilibrium conditions. Forcing the parameterized erosion ratio ($\hat{r}$) based on (15) does not necessarily change model skill but can erroneously attribute model variance to the "unknown" linear trend term (*b*) rather than to temporal gradients in the wave forcing.

Comparing the skill assessment for both the site-specific calibration (Table 4) and the parameterized form of the model at the original 12 sites, four of which were not used in the parameterization, eight sites remained skillful ($R \geq 0.7$; BSS $\geq$ 0.6; NMSE $\leq$ 0.4, and Table 5). All 12 of the parameterized model results were defined as minimum "good" based on BSS (Table 3) and five were ranked as "excellent" (Table 5) similar to the results of the site-specific calibrated versions (Table 4). NMSE increased (or remained the same) at all sites, with eight sites being ranked as "good" (Table 5) compared to 11 in the calibrated model results. Overall, the reduction of model coefficients by 2 is a significant improvement in the model with minimal loss of model skill, and therefore potentially increasing wider application of the equilibrium-based *ShoreFor* model at sites where insufficient data is available for calibration (refer to *Splinter et al.* [2013a, 2013b]). It is anticipated that the derived parameterizations, which were based on a minimum of 5 years of data, could be used to predict shorelines for 5–10 year simulations [*Splinter et al.*, 2013b], provided the wave climate was stationary (i.e., $\overline{\Omega}$ did not vary significantly over the timescales of a model run). For longer-term simulations, the ability for the response factor ($\hat{\phi}$ equation (13)) and the rate parameter ($\hat{c}$, equation (14)), to adjust to changes in $\overline{\Omega}$ and a time-varying linear trend term (*b*) is expected to improve model performance and will be a topic of future research.

Table 5. Skill Assessment of All Model Results Based on Parameterized Model (c and ϕ)[a]

Site	R	BSS	NMSE	Significant
North Head, WA	0.82	0.85	0.33	Y
Truc Vert, FR	0.83	0.84	0.32	Y
Gold Coast, QLD	0.80	0.80	0.36	Y
Ocean Beach, OB8, CA	0.80	0.81	0.37	Y
Ocean Beach, OB5, CA	0.71	0.80	0.51	Y
Duck, NC	0.63	0.61	0.66	N
Narrabeen, PF1, NSW	0.59	0.68	0.67	N
Narrabeen, PF2, NSW	0.57	0.69	0.74	N
Narrabeen, PF4, NSW	0.55	0.68	0.71	N
Narrabeen, PF6, NSW	0.80	0.74	0.36	Y
Narrabeen, PF8, NSW	0.78	0.69	0.40	Y
Narrabeen, 2600, NSW	0.82	0.76	0.34	Y
Torrey Pines, CA	0.80	0.85	0.37	Y

[a]Significant skill is defined as having an $R \geq 0.70$ and BSS ≥ 0.6.

To further test the generalized model, we introduce an additional shoreline data set that was not used in the previous model assessment or free parameter derivation. Torrey Pines is a fine-grained (d_{50} ~0.23 mm), microtidal (ΔTide = 1.62 m), sandy beach located at the southern end of an 82 km littoral cell in southern California [*Nordstrom and Inman*, 1975]. Torrey Pines shoreline data have been used recently by several researchers to develop and test equilibrium-based shoreline models [*Miller and Dean*, 2004a; *Yates et al.*, 2009]. The MSL shoreline positions over a 5 year period as presented in Figures 4 and 9 of *Yates et al.* [2009] were digitized and used here as a blind test case of an exposed beach that exhibits a strong seasonal signal in profile response related to changes in offshore wave conditions [e.g., *Aubrey*, 1979]. These digitized data were purposefully spaced at monthly intervals to avoid biasing correlation statistics for more closely sampled (weekly) surveys between May 2007 and May 2008 as is also presented in *Yates et al.* [2009].

Hourly wave data sourced from the deep water CDIP100 buoy was used to force the model, in place of the high-resolution (100 m alongshore-spaced) spectral refraction wave model output at the −10 m contour directly offshore of Torrey Pines utilized in *Yates et al.* [2009], which was not available to the present study. This site is the least energetic of the exposed sites ($\overline{\Omega} = 5.04$), but similar to the other sites has a large annual standard deviation in waves ($\overline{\sigma}_{\Omega_{360}} \sim 1.89$) that is observed in the annual cycle of shoreline variability. The ratio of $\overline{\sigma}_{\Omega_{360}}/\overline{\sigma}_{\Omega_{30}} = 1.14$ and is comparable to Gold Coast, resulting in $\overline{\Omega}_r = 5.75$. Model skill utilizing the parameterized forms of $\hat{\phi}$ (equation (13)) and $\hat{c}$ (equation (14)) when applied to the digitized Torrey Pines shoreline data was ranked as "good" to "excellent" ($R = 0.80$, BSS = 0.85, NMSE = 0.37, Table 5, and Figure 9).

While the sites used here for empirically derived versus site-specific model-model comparison are quite diverse in their characteristics and the parameterized model showed good skill on a blind test site, many of the same observations underpin the two approaches. What is now required is to further test and likely refine the empirical formulations of the response factor ($\hat{\phi}$, equation (13)) and the rate parameter ($\hat{c}$, equation (14)) presented here, using new survey data sets that may be available to other research teams. To assist this, a user-friendly (GUI-driven) version of the current *ShoreFor* model is available via the corresponding author.

6. Conclusions

Twelve shoreline data sets with suitable colocated wave data from a diverse range of beach sites were used to (1) calibrate and assess the generic applicability of the concept of wave-driven equilibrium shoreline response over timescales of weeks to a decade and (2) to further explore the dependence of the two wave-driven model coefficients on underlying environmental variables.

The concept of equilibrium-driven shoreline change was found to be most successful at exposed open coastlines, where a change in wave steepness is the predominant driving factor of shoreline change via onshore and offshore transport. The model reproduced the dominant seasonal cycle at five exposed sites with significant skill (BSS ≥ 0.80, Table 4). Semiembayed beaches are more likely to be influenced by gradients in longshore transport, as well as cross-shore processes and, therefore, the application of wave-driven equilibrium shoreline models based on cross-shore processes only are time and site dependent.

Across the 12 sites the model coefficients were found to be systematically related to the dimensionless fall velocity (Ω). The response factor (ϕ) was found to be highly dependent on the mean ($\overline{\Omega}$) and the mean standard deviation of Ω at yearly ($\overline{\sigma}_{\Omega_{360}}$) and monthly ($\overline{\sigma}_{\Omega_{30}}$) timescales. The rate parameter (c) was highly dependent on $\overline{\Omega}$. The empirical parameterizations for both terms ($\hat{c}$, $\hat{\phi}$) compared well with calibrated values ($R^2 \geq 0.99$) and were further utilized to test a generalized form of the model. The generalized form of

the model remained skillful (BSS $\geq$ 0.70) at eight sites over the 5+ years of data available, plus one additional "blind" test site that was not used in the initial analysis. While site-specific calibration is ideal, these new parameterizations can provide, at a minimum, initial estimates of model coefficients in methods such as those outlined in *Long and Plant* [2012] and perhaps also reducing the further need for extensive shoreline data sets to inform site-specific calibration.

Acknowledgments

This research was made possible with the help and data provided by many people, specifically the Argus user group who has provided the foundation and maintenance of numerous coastal imaging sites around the world. K.D.S. particularly wishes to thank R. Holman and J. Stanley of the Coastal Imaging Lab (CIL, Oregon State University) for their continued support in all things Argus and for always pushing her to think harder. The CIL is funded in part by the Office of Naval Research, N00014-10-1-0046. Argus-derived shoreline data from North Head, WA, USA were supplied by NWRA with funding from U.S. Army Corps of Engineers Portland District. Gold Coast and Narrabeen Argus-derived shorelines were provided by the UNSW Australia, Water Research Laboratory in partnership with Warringah Council and Gold Coast City Council. Profile data from Duck, NC were obtained from the U.S. Army Corps of Engineers Field Research Facility (FRF). Beach Surveys at Truc Vert were funded by SOLAQUI and Region Aquitaine. K.D.S. wishes to thank J.K. Miller for providing historical data for Torrey Pines and Duck in the initial stages of this work. Wave data were obtained from Manly Hydraulics Laboratory, Gold Coast City Council, the FRF, NOAA and CDIP buoys, WWIII (Truc Vert), and SWAN modeling from E. Kearney and J. Hansen (USGS). Funding for K.D.S. was provided under ARC Linkage project LP100200348 with support from NSW Office of Environment and Heritage, Warringah Council and CoastalCOMS. M.A.D. would like to thank the Plymouth Universities' Marine Institute for financial support for his sabbatical that made this work possible and a special thanks to UNSW Australia, School of Civil and Environmental Engineering for funding and hosting his visits to work with the Australian team. B.C. is funded by project BARBEC (ANR N2010 JCJC 60201). The GUI was developed by T. Beuzen under the direction of K.D.S. and I.L.T and funded by a UNSW Australia, School of Civil and Environmental Engineering Elite Student Scholarship.

References

Alexander, P. S., and R. A. Holman (2004), Quantitative analysis of nearshore morphological variability based on video imaging, *Mar. Geol.*, *208*(1), 101–111.

Allen, M., and J. Callaghan, (1999), Extreme wave conditions for the South Queensland coastal region, *Report*, EPA, Queensland.

Anderson, T. R., L. N. Frazer, and C. H. Fletcher (2010), Transient and persistent shoreline change from a storm, *Geophys. Res. Lett.*, *37*, L08401, doi:10.1029/2009GL042252.

Aubrey, D. G. (1979), Seasonal patterns of onshore/offshore sediment movement, *J. Geophys. Res.*, *84*, 6347–6354.

Barnard, P., J. E. Hansen, and L. H. Erikson (2012), Synthesis study of an erosion hot spot, Ocean Beach, California, *J. Coastal Res.*, *28*(4), 903–922.

Birkemeier, W. A., H. C. Miller, S. D. Wilhelm, A. E. DeWall, and C. S. Gorbics, (1985), User's guide to CERC's Field Research Facility, *Tech. Rep. Instruction Report-85-1*, Coastal Eng. Res. Cent., Field Res. Fac., U. S. Army Eng. Waterw. Exp. Sta., Vicksburg, Miss.

Callaghan, D. P., P. Nielsen, A. Short, and R. Ra (2008), Statistical simulation of wave climate and extreme beach erosion, *Coastal Eng.*, *55*, 375–390.

Carley, J. T., I. L. Turner, E. D. Couriel, L. A. Jackson, and J. E. McGrath (1999), The practical application of four commercially available numerical beach morphology models on a high energy coastline, in *Proceedings of the Australian Coastal and Ocean Engineering Conference,* Perth, AU, pp. 101–106.

Castelle, B., P. Bonneton, H. Dupuis, and N. Senechal (2007a), Double bar beach dynamics on the high-energy meso-marcotidal French Aquatian Coast: A review, *Mar. Geol.*, *245*, 141–159.

Castelle, B., I. Turner, B. G. Ruessink, and R. Tomlinson (2007b), Impact of storms on beach erosion: Broadbeach (Gold Coast, Australia), *J. Coastal Res.*, *SI50*, 534–539.

Castelle, B., V. Marieu, S. Bujan, S. Ferreira, J.-P. Parisot, S. Capo, N. Senechal, and T. Chouzenoux (2014), Equilibrium shoreline modelling of a high-energy meso-macrotidal multiple-barred beach, *Mar. Geol.*, *347*, 84–94.

Clarke, D., and I. Eliot (1988), Low-frequency changes of sediment volume on the beachface at Warilla Beach, New South Wales, 1975–1985, *Mar. Geol.*, *79*, 189–211, doi:10.1016/0025-3227(88)90039-4.

Davidson, M., I. Turner, and R. Guza (2011), The effect of temporal wave averaging on the performance of an empirical shoreline evolution model, *Coastal Eng.*, *58*, 802–805.

Davidson, M. A., and I. L. Turner (2009), A behavioral template beach profile model for predicting seasonal to interannual shoreline evolution, *J. Geophys. Res.*, *114*, F01020, doi:10.1029/2007JF000888.

Davidson, M. A., R. P. Lewis, and I. L. Turner (2010), Forecasting seasonal to multi-year shoreline change, *Coastal Eng.*, *57*, 620–629, doi:10.1016/j.coastaleng.2010.02.001.

Davidson, M. A., K. D. Splinter, and I. L. Turner (2013), A simple equilibrium model for predicting shoreline change, *Coastal Eng.*, *73*, 191–202, doi:10.1016/j.coastaleng.2012.11.002.

Dean, R. G. (1973), Heuristic models of sand transport in the surf zone, in *Proceedings of the 1st Australian Cong. on Coastal Eng., Conference on Engineering Dynamics in the Surf Zone,* pp. 209–214, Sydney, Australia.

Delft, (1970), Gold Coast, Queensland, Australia—Coastal erosion and related problems, *Tech. Rep. R257*, Delft Hydraulics Laboratory, Delft, The Netherlands.

Eshleman, J. L., P. L. Barnard, L. H. Erikson, and D. M. Hanes (2007), Coupling alongshore variations in wave energy to beach morphologic change using the SWAN wave model at Ocean Beach, San Francisco, CA, *10th International Workshop on Wave Hindcasting and Forecasting and Coastal Hazard Symposium,* p. 20, North Shore, Oahu, Hawaii.

Frazer, L. N., T. R. Anderson, and C. H. Fletcher (2009), Modeling storms improves estimates of long-term shoreline change, *Geophys. Res. Lett.*, *36*, L20404, doi:10.1029/2009GL040061.

Hansen, J., E. Elias, and P. Barnard (2013a), Changes in surf zone morphodynamics driven by multi-decadal contraction of a large ebb-tidal delta, *Mar. Geol.*, *345*, 221–234, doi:10.1016/j.margeo.2013.07.005.

Hansen, J., E. Elias, J. List, L. Erikson, and P. Barnard (2013b), Tidally influenced alongshore circulation at an inlet-adjacent shoreline, *Cont. Shelf Res.*, *56*, 26–38, doi:10.1016/j.csr.2013.01.017.

Hansen, J. E., and P. L. Barnard (2010), Sub-weekly to interannual variability of a high-energy shoreline, *Coastal Eng.*, *57*, 959–972, doi:10.1016/j.coastaleng.2010.05.011.

Hanson, H., and N. Kraus, (1989), Generalized model for simulating shoreline change, *Report 1, Technical Reference, Tech. Rep.*, U. S. Army Engineer Waterways Experiment Station; Coastal Engineering Research Center (U. S.); United States. Army. Corps of Engineers.

Harley, M. D., I. L. Turner, A. D. Short, and R. Ranasinghe (2011), A re-evaluation of coastal embayment rotation: The dominance of cross-shore versus alongshore sediment transport processes, Collaroy-Narrabeen Beach, SE Australia, *J. Geophys. Res.*, *116*, F04033, doi:10.1029/2011JF001989.

Holman, R., J. Stanley, and H. Özkan Haller (2003), Applying video sensor networks to nearshore environmental monitoring, *IEEE Pervasive Comput.*, *2*(4), 14–21.

Idier, D., B. Castelle, E. Charles, and C. Mallet (2013), Longshore sediment flux hindcast: Spatio-temporal variability along the SW Atlantic coast of France, *J. Coastal Res.*, *SI65*, 1785–1790.

Karunarathna, H., and D. E. Reeve (2013), A model for beach plan shape change using an inverse approach, *Coastal Dynamics 2013,* France, pp. 937–946.

Komar, P. D. (1974), *Beach Processes and Sedimentation*, Prentice-Hall, Englewood Cliffs, N. J.

Larson, M., and N. Kraus, (1989), SBEACH: Numerical model for simulating storm-induced beach change; Report 1, Empirical foundation and model development, *Tech. Rep. CERC 89-9*, Coastal Engineering Research Center, Vicksburg, Miss.

Lippmann, T., and R. Holman (1990), The spatial and temporal variability of sand bar morphology, *J. Geophys. Res.*, *95*(C7), 11,575–11,590.

List, J. H., A. S. Farris, and C. Sullivan (2006), Reversing storm hotspots on sandy beaches: Spatial and temporal characteristics, *Mar. Geol.*, *226*, 261–279.

Long, J. W., and N. G. Plant (2012), Extended Kalman Filter framework for forecasting shoreline evolution, *Geophys. Res. Lett.*, *39*, L13603, doi:10.1029/2012GL052180.
McCall, R. T., J. S. M. Van Thiel de Vries, N. G. Plant, A. R. Van Dongeren, J. A. Roelvink, D. M. Thompson, and A. J. H. M. Reniers (2010), Two-dimensional time dependent hurricane overwash and erosion modeling at Santa Rosa Island, *Coastal Eng.*, *57*, 668–683.
Miller, J. K., and R. G. Dean (2003), Implications of longshore variability in shoreline change modeling, in *Proceedings of Coastal Sediments 2003*, pp. 1–14, World Scientific and East Meets West Productions, Corpus Christi, Tex.
Miller, J. K., and R. G. Dean (2004a), A simple new shoreline change model, *Coastal Eng.*, *51*, 531–556.
Miller, J. K., and R. G. Dean (2004b), A simple new shoreline evolution model, in *Proceedings of the 29th International Conference on Coastal Engineering*, vol. 2, edited by J. M. Smith, pp. 2009–2021, ASCE, World Scientific Publishing, Lisbon, Portugal.
Nordstrom, C. E., and D. L. Inman, (1975), Sand level changes on Torrey Pines Beach, California, *MP 11-75*, U. S. Army Corps Engineers, Coastal Engineering Research Center, Fort Belvoir, Va.
Patterson, D. (2007), Sand transport and shoreline evolution, Northern Gold Coast, Australia, *9th International Coastal Symposium,* Gold Coast, Australia, pp. 147–151.
Pelnard-Considere, R. (1956), Essai de theorie do l'evolution des forms de rivageen plage de sable et de galets, *4me Journees de l'Hydraulique, Les Energies de la Mer, Question III, Rapport No. 1*, pp. 289–298, Societe Hydrotechnique de France, Paris, France.
Pender, D., and H. Karunarathna (2013), A statistical-process based approach for modelling beach profile variability, *Coastal Eng.*, *81*, 19–29, doi:10.1016/j.coastaleng.2013.06.006.
Plant, N., R. Holman, and M. Freilich (1999), A simple model for interannual sand bar behavior, *J. Geophys. Res.*, *104*(C7), 15,755–15,776.
Plant, N. G., and R. A. Holman (1996), Interannual shoreline variations at Duck, NC, USA, in *Proceedings of the 25th International Conference On Coastal Engineering*, pp. 3521–3533, ASCE, Orlando, Fla.
Ranasinghe, R., R. McLoughlin, A. Short, and G. Symonds (2004), The Southern Oscillation Index, wave climate, and beach rotation, *Mar. Geol.*, *204*, 273–287, doi:10.1016/S0025-3227(04)00002-7.
Roelvink, D., A. Reniers, A. van Dongeren, J. van Thiel de Vries, R. McCall, and J. Lescinski (2009), Modelling storm impacts on beaches, dunes and barrier islands, *Coastal Eng.*, *56*(11-12), 1133–1152, doi:10.1016/j.coastaleng.2009.08.006.
Ruessink, B., L. Pape, and I. Turner (2009), Daily to interannual cross-shore sandbar migration: Observations from a multiple sandbar system, *Cont. Shelf Res.*, *29*, 1663–1677.
Ruggiero, P., D. Walstra, G. Gelfenbaum, and M. van Ormondt (2009), Seasonal-scale nearshore morphological evolution: Field observations and numerical modeling, *Coastal Eng.*, *56*(11-12), 1153–1172, doi:10.1016/j.coastaleng.2009.08.003.
Ruggiero, P., M. Buijsman, G. M. Kaminsky, and G. Gelfenbaum (2010), Modeling the effects of wave climate and sediment supply variability on large-scale shoreline change, *Mar. Geol.*, *273*(1-4), 127–140, doi:10.1016/j.margeo.2010.02.008.
Senechal, N., T. Gouriou, B. Castelle, J.-P. Parisot, S. Capo, S. Bujan, and H. Howa (2009), Morphodynamic response of a meso- to macro-tidal intermediate beach based on a long-term data set, *Geomorphology*, *107*, 263–274.
Short, A. D., and A. C. Trembanis (2004), Decadal scale patterns in beach oscillation and rotation Narrabeen Beach, Australia—Time series, PCA, and wavelet analysis, *J. Coastal Res.*, *20*(2), 523–532.
Splinter, K. D., and M. L. Palmsten (2012), Modeling dune response to an East Coast Low, *Mar. Geol.*, *329-331*, 46–57, doi:10.1016/j.margeo.2012.09.005.
Splinter, K. D., R. Holman, and N. Plant (2011a), A behavior-oriented dynamic model for sand bar migration and 2DH evolution, *J. Geophys. Res.*, *116*, C01020, doi:10.1029/2010JC006382.
Splinter, K. D., D. Strauss, and R. Tomlinson (2011b), Assessment of post-storm recovery of beaches using video imaging techniques: A case study at Gold Coast, Australia, *IEEE Trans. Geosci. Remote Sens.*, *49*(12), 4704–4716, doi:10.1109/TGRS.2011.2136351.
Splinter, K. D., M. A. Davidson, A. Golshani, and R. B. Tomlinson (2012), Climate controls on longshore sediment transport, *Cont. Shelf Res.*, *48*, 146–156, doi:10.1016/j.csr.2012.07.018.
Splinter, K. D., M. A. Davidson, and I. L. Turner (2013a), Monitoring data requirements for shoreline prediction: How much, how long, how often, in *Proceedigs of the 12th International Coastal Symposium (Plymouth England), Journal of Coastal Research*, vol. SI 65, edited by D. C. Conley et al., pp. 2179–2184, Coconut Creek, Fla.
Splinter, K. D., I. L. Turner, and M. A. Davidson (2013b), How much data is enough? The importance of morphological sampling interval and duration for calibration of empirical shoreline models, *Coastal Eng.*, *77*, 14–27, doi:10.1016/j.coastaleng.2013.02.009.
Splinter, K. D., J. T. Carley, A. Golshani, and R. Tomlinson (2014), A relationship to describe the cumulative impact of storm clusters on beach erosion, *Coastal Eng.*, *83*, 49–55, doi:10.1016/j.coastaleng.2013.10.001.
Sutherland, J., and R. L. Soulsby (2003), Use of model performance statitics in modelling coastal morphodynamics, in *Proceedings of Coastal Sediments '03*, vol. CD-ROM, pp. 1–14, World Scientific Co., East Meets West Productions, Corpus Christi, Tex. [Available at http://www.worldscientific.com/worldscibooks/10.1142/5315.]
van de Lageweg, W., K. Bryan, G. Coco, and B. Ruessink (2013), Observations of shoreline-sandbar coupling on an embayed beach, *Mar. Geol.*, *344*, 101–114, doi:10.1016/j.margeo.2013.07.018.
van Enckevort, I., B. Ruessink, G. Coco, K. Suzuki, I. Turner, N. Plant, and R. A. Holman (2004), Observations of nearshore crescentic sandbars, *J. Geophys. Res.*, *109*, C06028, doi:10.1029/2003JC002214.
van Rooijen, A., A. Reniers, J. van Thiel de Vries, C. Blenkinsopp, and R. McCall (2012), Modeling swash zone sediment transport at Truc Vert Beach, in *Proceedings of the 33rd Conference on Coastal Engineering*, edited by P. Lynett and J. M. Smith, ASCE, Santander, Spain.
Wright, L. D., and A. D. Short (1984), Morphodynamic variability of surf zones and beaches: A synthesis, *Mar. Geol.*, *56*, 93–118.
Wright, L. D., A. D. Short, and M. O. Green (1985), Short-term changes in the morphodynamic states of beaches and surf zones: An empirical predictive model, *Mar. Geol.*, *62*, 339–364.
Yates, M. L., R. T. Guza, and W. C. O'Reilly (2009), Equilibrium shoreline response: Observations and modeling, *J. Geophys. Res.*, *114*, C09014, doi:10.1029/2009JC005359.
Yates, M. L., R. T. Guza, W. C. O'Reilly, J. E. Hansen, and P. L. Barnard (2011), Equilibrium shoreline response of a high wave energy beach, *J. Geophys. Res.*, *116*, C04014, doi:10.1029/2010JC006681.